E-155

A Proposal for

MEASUREMENTS OF NUCLEON SPIN STRUCTURE AT SLAC IN END STATION A

Co-spokesmen: R. Arnold, J. McCarthy

R. Arnold, P. Bosted, J. Dunne, J. Fellbaum, S. Rock
D. Reyna, Z. Szalata, J. White
American University, Washington D. C. 20016

A. Feltham, D. Fritschi, J. Jourdan, G. Masson
S. Robinson, I. Sick, P. Steiner
Institut für Physik der Universität, CH 4056 Basel, Switzerland

J. Gomez, J. Mitchell, S. Nanda
CEBAF, Newport News, VA 23606

H.Borel, R. Lombard-Nelson, J. Marroncle, F. Staley, Y. Terrien
Centre d'Etudes Physique de Saclay, Gif sur Yvette, France

P. Bertin, V. Breton, H. Fonvieille
LPC IN2P3/CNRS, University Blaise Pascal, Clermont-Ferrand, France

P. Degtyarenko, S. Shuvalov
ITEP, Moscow Russia

F. Dietrich
Lawrence Livermore National Laboratory, Livermore, CA 94550

J. Bauer, J. Button-Shafer, L. Elouadrhiri, R. Hicks,
R. Miskimen, G. Peterson, K. Wang
University of Massachusetts, Amherst, MA 00013

T. Chupp
University of Michigan, Ann Arbor, MI 48109-1120

C. Hyde-Wright, A. Klein, S. Kuhn
Old Dominion University, Norfolk, VA 23529

P. Anthony, J. Clendenin, H. Dutz, R. Erbacher, R. Gearhart,
E. Hughes, T. Maruyama, W. Meyer, G. Petratos,
R. Pitthan, C. Prescott, L. Rochester, L. M. Stuart
S. St. Lorant, H.Tang, K. Witte, C. Young
Stanford Linear Accelerator Center, Stanford University, Stanford, CA 94309

P. Decowski
Smith College, Northampton MA 01063

K. Abe, T. Akagi, F. Suekane, H. Yuta
Tohoku University

T. Averett, C. Cothran, D. Crabb, D. Day, E. Frlez, R. Gladyshev
S. Iløibråten, R. Lindgren, T. Liu, R. Lourie, J. McCarthy, P. McKee,
R., Minehart, D. Pocanic, O. Rondon-Aramayo, C. Smith, S. VanVerst
University of Virginia, Charlottesville, VA 22901

K. Griffioen, R. Antonov, P. Raines
The College of William and Mary, Williamsburg, VA 23185
and
University of Pennsylvania, Philadelphia, PA 19104

H. Band, J. Johnson, R. Prepost, G. Zapalac
University of Wisconsin, Madison, WI 53706

ABSTRACT

This proposal is for a series of precision measurements of deep inelastic scattering of polarized electrons from polarized ammonia targets (NH3 and ND3) to determine the spin structure functions g_1 and g_2 of the proton and neutron over a range in Bjorken scaling variable $0.015 \leq x \leq 0.85$ and momentum transfer $1 \leq Q^2 \leq 17$ (Gev/c)^2. This will extend x the range of precision spin structure measurements, cutting in half the unmeasured region near $x = 0$ and significantly extending the range near $x = 1$. This data will double the Q^2 range of precision measurements and allow a search for non-scaling higher-twist contributions to the spin structure functions. With careful attention to systematic errors, with measurements of contributions from g_2 in transverse asymmetries, and with measurements of possible higher-twist contributions, this data will allow precision tests of the sum rules for integrals over the g_1 structure functions. The Ellis-Jaffe sum rule $\int g_1^p(x)dx$ will be tested to $\pm 0.0011(\pm 0.0077)$ statistal (systematic) error, and the integral $\int g_1^n(x)dx$ will be tested to $\pm 0.0023(\pm 0.0062)$ statistical (systematic) error. The Bjorken sum rule $\int (g_1^p(x) - g_1^n(x))dx$ will be tested to $\pm 0.0030(\pm 0.0115)$ which is $\pm 1.6\%(\pm 6.4\%)$ if the sum is 0.18.

The measurements will be made in SLAC End Station A using a beam of polarized electrons at 48.55 GeV with polaraization $Pb \sim 0.8$. A new pair of focussing magnetic spectrometers instrumented with shower counters, Čerenkov counters, and scintillator hodoscopes to measure scattered electrons and reject pions are proposed. Three calendar months of beam for data taking will be required.

The main request to SLAC is for approval to build the new spectrometer and detector systems described here and to run for three calendar months for physics data.

CONTENTS

I. INTRODUCTION

Measurements of the nucleon spin structure functions are necessary to provide fundamental tests of QCD and the quark structure of hadrons. Deep inelastic electron or muon scattering with polarized beams and polarized targets directly probes the distribution of the spin on the nucleon quark constituents. The data can be used to extract the proton and neutron spin structure functions, $g_1(x)$ and $g_2(x)$, for a direct test of quark models of nucleon structure. In addition the data can be used to test a number of sum rules based on various integrals of $g_1(x)$ and $g_2(x)$ over x, the Bjorken scaling variable. The most important of these is the Bjorken sum rule[1] which relates the integral of $g_1(x)$ for the proton and neutron to a number measured in neutron beta decay. The Bjorken sum rule is based on current algebra and a few fundamental principles at the root of QCD and the standard model. Bjorken has said "If the Bj sum rule is wrong then QCD is wrong." Therefore it must be tested.

Ellis and Jaffe have written two other sum rules[2] for the separate integrals over $g_1(x)$ of the proton and neutron that are also related to some numbers measured in weak decays. The Ellis-Jaffe sum rules are derived with some model-dependent assumptions, and therefore are less fundamental than the Bjorken sum rule. However they provide powerful constraints for testing nucleon structure.

In the past several years a new generation of experiments by SMC[3,4] at CERN and by E142[5] (and soon by E143) at SLAC have provided (or will provide) new data that considerably extend the previous limited results from EMC[6] and SLAC[7,8] more than a decade ago. These new data offer the chance to observe the spin distributions with some precision and enough kinematic coverage to begin effective tests of the sum rules. The evidence is not all in yet, with more data still to come from SMC and E143, but the experimental situation is far from satisfactory. The proton $g_1^p(x)$ measurements from EMC and earlier SLAC experiments disagree with the Ellis-Jaffe sum rule, and this can be interpreted as evidence that the spin in the proton is not carried by the quarks. These data have generated

wide interest, and a huge number of theoretical papers have been produced seeking to understand the result. Recent results from SMC using a deuteron target and E142 using a ^{3}He target give the first look at the neutron spin. The data indicate that $g_1^n(x)$ is small and negative at low x. Within the errors (large for SMC) the experiments are consistent. Using the SLAC-EMC proton data together with the Bjorken sum rule gives a prediction for $g_1^n(x)$ that is 1.5σ from the E142 result.

Before we can say with confidence that the Bjorken sum rule is or is not satisfied, we clearly need more extensive and accurate data. Data with small errors are needed at low and high x to reduce the uncertainty from extrapolation of the sum rule integrals to $x = 0$ and $x = 1$. Any possible non-scaling behavior versus Q^2 must be ruled out, and the reliability of extracting the neutron spin structure from data on nuclear targets must be tested.

With the intense and highly polarized electron beam up to 50 GeV now available at SLAC, with improved spectrometer facilities in End Station A, and with the polarized targets now tested or under construction, it will be possible in the next few years to measure the spin structure functions with sufficient coverage in x and Q^2 and with errors small enough to test the sum rules to the level of 5% to 10%. The first step in that process will be the completion of experiment E143 using a polarized ammonia (proton and deuterated) to measure proton and neutron $g_1(x)$ and $g_2(x)$. E143 is optimized with spectrometer angles and detector configurations to measure in the range $0.03 \leq x \leq 0.7$ and $1 \leq Q^2 \leq 7$ (GeV/c)^2 using beam energies of 9 and 29 GeV.

A further step in the experimental program of spin structure functions at SLAC is presented in this proposal. We propose to extend the measurements of proton and neutron spin beyond those to be done by E143 in three important areas:

1. by cutting the unmeasured region at low x in half and extending the measurements to significantly higher x,
2. by doubling the Q^2 range, and
3. by reducing the experimental errors.

The measurements we propose will cover the kinematic range $0.015 < x < 0.85$ and $1 < Q^2 < 17$ (GeV/c)^2 with small errors. Measurements with small errors are essential for testing the sum rules, especially at low x, to reduce the error on the extrapolation to the unmeasured region in x.

Measurements over a range of Q^2 are necessary to test whether the spin structure functions obey scaling in the SLAC kinematic region. The Bjorken sum rule and Ellis-Jaffe sum rules require that scaling be valid. If it is discovered that the structure functions do not obey scaling and have a Q^2 dependence different from that expected from the normal QCD evolution plus target mass effects due to the presence of non-scaling higher twist terms, then the Q^2-dependent measurements will allow for corrections to be made so that the sum rules can be properly tested. The spin-averaged structure functions from unpolarized scattering show significant contributions from higher twist terms in the range $1 \leq Q^2 \leq 10$ (GeV/c)^2. Observation of non-scaling behavior of the spin structure functions would be important information needed for a complete understanding of the nucleon structure.

For the neutron we will always have the special problem of extracting reliable spin structure functions from scattering on polarized nuclear targets. We know from unpolarized scattering measurements that there are significant nuclear effects (generally referred to as the EMC effect) on the structure functions in the region $x \geq 0.2$ due to the distortion of the quark momenta from nuclear binding and for $x \leq 0.2$ from nuclear shadowing. Before we can say with confidence that we have extracted the spin structure appropriate for a free neutron we will have to demonstrate by measurements that we get the same results from different nuclear targets. Measurements of neutron spin structure with comparable accuracy from both deuterium and ^{3}He targets will be essential for this test.

To accomplish these goals we propose to make a number of changes to the experimental plan from those to be used by E143:

1. The beam energy will be raised to 48.55 GeV. This is the primary means for extending the x and Q^2 range.

2. The spectrometers will be optimized in scattering angle and optics for maximum solid angle while maintaining adequate background rejection and resolution for measurements at 48.6 GeV.

3. A new detector system that identifies scattered electrons but avoids the large background of low energy particles and pions will be assembled. It will employ Čerenkov counters and lead glass shower counters for electron identification, and scintillator hodoscopes for tracking.

While we are convinced that the resources required for this experiment in beam time, spectrometers, and equipment are worth the investment, we are also aware that SLAC has limited resources and that our plans must be economical. Therefore the plan in this proposal has been made with the following considerations in mind:

1. The spectrometer and detector packages make extensive use of existing equipment. Most of the major items (magnets, shielding, Čerenkov tanks, much of the lead glass) exist at SLAC. Some new equipment will be required.

2. The spectrometer and detector systems are compatible with measurements of the neutron spin structure using the E142 style polarized ^{3}He target. In Appendix C we show the possible results for the neutron structure function using a He target and the proposed spectrometers and detectors.

The following sections give more details on the physics and the experiment. The main request to SLAC is for approval to build the new spectrometer and detector systems described here and to run for three calendar months for physics data.

II. PHYSICS MOTIVATION

Definitions

In inclusive polarized-lepton scattering from polarized nucleons, the total deep-inelastic cross section can be split into symmetric and antisymmetric components. The symmetric part of the cross section is just the unpolarized cross section which

in the laboratory frame is given by

$$\frac{d^2\sigma}{d\Omega dE'} = \sigma = \sigma_{Mott}\Big[\frac{1}{\nu}F_2(\nu,Q^2) + \frac{2}{M}F_1(\nu,Q^2)\tan^2(\theta/2)\Big]. \tag{1}$$

Here, $\nu = E - E'$, E and E' are the initial and final lepton energies, Ω is the detector solid angle, M is the nucleon mass, Q^2 is the four-momentum transfer squared, θ is the lepton scattering angle, $F_1(\nu,Q^2)$ and $F_2(\nu,Q^2)$ are the unpolarized structure functions, and $\sigma_{Mott} = 4\alpha^2 E'^2\cos^2(\theta/2)/Q^4$.

The antisymmetric part of the cross section is the embodiment of the nucleon spin structure functions, and its sign depends on the helicity of the nucleon relative to that of the incident lepton. The difference in cross sections with different helicity orientations[9,10] is sensitive to only the polarized part of the nucleon structure. For longitudinally polarized electrons and nucleons we have

$$\frac{d^2\sigma^{\uparrow\downarrow}}{d\Omega dE'} - \frac{d^2\sigma^{\uparrow\uparrow}}{d\Omega dE'} = \sigma^{\uparrow\downarrow} - \sigma^{\uparrow\uparrow} = \frac{4\alpha^2 E'}{Q^2 E}\Big[(E + E'\cos\theta)MG_1(\nu,Q^2) - Q^2 G_2(\nu,Q^2)\Big], \tag{2}$$

and for longitudinally polarized leptons and transversely polarized nucleons the result is

$$\frac{d^2\sigma^{\uparrow\leftarrow}}{d\Omega dE'} - \frac{d^2\sigma^{\downarrow\leftarrow}}{d\Omega dE'} = \sigma^{\uparrow\leftarrow} - \sigma^{\downarrow\leftarrow} = \frac{4\alpha^2 E'}{Q^2 E}E'\sin\theta\Big[MG_1(\nu,Q^2) + 2EG_2(\nu,Q^2)\Big], \tag{3}$$

where $G_1(Q^2,\nu)$ and $G_2(Q^2,\nu)$ are the spin structure functions. The sum of the polarized cross sections is just twice the unpolarized cross section, $2\sigma = \sigma^{\uparrow\downarrow} + \sigma^{\uparrow\uparrow} = \sigma^{\uparrow\leftarrow} + \sigma^{\downarrow\leftarrow}$. In the asymptotic scaling limit the polarized and unpolarized structure functions are expressed in terms of a single variable, $x = Q^2/(2M\nu)$,

$$\begin{aligned} &\lim_{Q^2,\nu\to\infty} M^2\nu G_1(\nu,Q^2) = g_1(x), && \lim_{Q^2,\nu\to\infty} M\nu^2 G_2(\nu,Q^2) = g_2(x), \\ &\lim_{Q^2,\nu\to\infty} F_1(\nu,Q^2) = F_1(x), && \lim_{Q^2,\nu\to\infty} F_2(\nu,Q^2) = F_2(x). \end{aligned} \tag{4}$$

It can be shown from Equations (1-4) and the definition for the longitudinal

asymmetry, $A^{\parallel} = (\sigma^{\uparrow\downarrow} - \sigma^{\uparrow\uparrow})/(2\sigma)$, that in the asymptotic limit,

$$g_1(x) - kg_2(x) = 2KA^{\parallel}\sigma/\sigma_{Mott}, \tag{5}$$

where the kinematical factors are defined by $K = EE'\cos^2(\theta/2)/[2x(E+E'\cos\theta)]$, and $k = 2xM/(E+E'\cos\theta)$. For $E = 49$ GeV, $k < 0.02$, so $A^{\parallel}$ essentially measures g_1. Similarly for the the transverse asymmetry, $A^{\perp} = (\sigma^{\uparrow\leftarrow} - \sigma^{\downarrow\leftarrow})/(2\sigma)$,

$$g_1(x) + k'g_2(x) = 2K'A^{\perp}\sigma/\sigma_{Mott}, \tag{6}$$

where $K' = E\cos^2(\theta/2)/(2x\sin\theta)$, and $k' = 2E/(E-E')$. $A^{\perp}$ primarily measures g_2.

The above equations can be solved to give g_1 and g_2 in terms of the cross section $\sigma(E, E', \theta)$ and the measured asymmetries $A^{\parallel}$ and $A^{\perp}$:

$$g_1 = \frac{\sigma}{\sigma_{Mott}} \; \frac{My}{2(2-y)\tan^2(\theta/2)} \; \left[A^{\parallel} + \tan(\theta/2)A^{\perp}\right] \tag{7}$$

$$g_2 = \frac{\sigma}{\sigma_{Mott}} \; \frac{My}{2(2-y)\tan^2(\theta/2)} \; \frac{y}{2\sin(\theta)} \; \left[\frac{[E+E'\cos(\theta)]}{E'}A^{\perp} - \sin(\theta)A^{\parallel}\right], \tag{8}$$

where $y = \nu/E$. Note that the relative contribution of $A^{\perp}$ to g_1 is suppressed by a constant factor of $\tan(\theta/2)$, and that the relative contribution of $A^{\parallel}$ to g_2 is suppressed by $\sin(\theta)$. Since θ is small for this proposal, g_1 is primarilly measured by $A^{\parallel}$, and g_2 is primarily measured by $A^{\perp}$.

It has been conventional in the past to express asymmetry measurements in terms of the virtual photon-nucleon asymmetries, $A_1(x)$ and $A_2(x)$. Expressions relating the A_1 and A_2 to the measured $A^{\parallel}$ and $A^{\perp}$ and kinematic factors containing $R = \sigma_L/\sigma_T$ are given in Appendix A. In the past it has also been necessary to neglect the contributions due to the A_2 because transverse asymmetries were not measured. In this proposal we follow Anselmino and Leader[11] and extract the structure functions $g_1(x)$ and $g_2(x)$ directly from measurements of $A^{\parallel}$, $A^{\perp}$ and σ using Equations (7)and (8).

Sum Rules

Theoretically, various sum rules have been established for integrals over the proton and neutron spin g_1 structure functions. The Bjorken sum rule[1] is a prediction derived from current algebra. With QCD corrections, the Bjorken sum rule is is given by

$$\int (g_1^p - g_1^n)dx = \frac{1}{6}\frac{g_A}{g_V}\left[1 - \frac{\alpha_s(Q^2)}{\pi} - \frac{43\alpha_s^2(Q^2)}{12\pi^2}\right], \tag{9}$$

where the ratio of the weak coupling constants found from beta decay measurements is $g_A/g_V = 1.254 \pm 0.006$, and the terms containing $\alpha_s(Q^2)$, the strong coupling constant, are the QCD correction for finite Q^2. For $\alpha_s(Q^2) = 0.33 \pm 0.02$ the Bjorken sum rule is predicted to be 0.179 ± 0.002.

The Ellis-Jaffe sum rules,[2] based on SU(3) symmetry, for the proton and neutron separately, and assuming that the nucleon does not contain polarized strange quarks, are given by[12]

$$\begin{aligned} \int g_1^p(x)dx &= \frac{1}{18}(9F - D)(1 - \alpha_s(Q^2)/\pi) = 0.170 \pm 0.018, \\ \int g_1^n(x)dx &= \frac{1}{18}(6F - 4D)(1 - \alpha_s(Q^2)/\pi) = -0.021 \pm 0.011, \end{aligned} \tag{10}$$

where $F = 0.47 \pm 0.04$ and $D = 0.81 \pm 0.03$ are weak coupling constants measured in beta decay. From Eq. (9)and Eq. (10) we get $F + D = g_A/g_V = 1.28$.

The "transverse" structure function, g_2, has also been the focus of theoretical study over the years. Fundamentally $g_2(x)$ originates from the transverse motion and spin distributions of the quarks. The origin is similar to the processes which gives rise to σ_L in the spin-averaged structure functions. At very large Q^2 the function $g_2(x)$ is expected to be small compared to $g_1(x)$, but for the Q^2 at SLAC $g_1(x)$ and $g_2(x)$ may be comparable in size.[13] The contribution of $g_2(x)$ to $A^{\|}$ is reduced by kinematic factors. However, measurements of $A^{\perp}$ are essential to reduce the uncertainty in extracting $g_1(x)$ from $A^{\|}$.

Measurements of $g_2(x)$, even if they are of limited precision, are interesting in their own right for information on the transverse spin distributions. Sum rules for g_2 have been developed by Burkhardt and Cottingham,[14] Wandzura and Wilczek,[15] and Belyaev and Ioffe.[16] Also, it has been suggested by the analyses of Leader and Anselmino[11] and Heimann[17] that there is a possible divergence of $g_2(x)$ at small x. This possiblility makes a measurement of g_2 especially appealing at small x. Recent studies by Jaffe and Ji[18] suggest that twist-3 contributions, reflecting quark-gluon interactions, are significant in $g_2(x)$, and that its measurement would be a unique opportunity to study them.

Q^2-Dependence

What about the Q^2 dependence of the spin structure functions? For a valid test of the sum rules the spin structure data must be in the scaling region. The QCD corrections to the sum rules due to the normal QCD evolution of the spin structure functions via the Alterelli-Parisi equations are expressed by $\alpha_s(Q^2)/\pi$ terms in Equations (9)and (10). Measurements made at different Q^2 need to be adjusted to some common Q^2 before taking the integral over x. Since the spin-averaged functions F_1 and F_2 and the spin-difference functions g_1 and g_2 all depend on the same QCD operators and splitting functions, we expect the QCD evolution of g_1 and g_2 will have a similar shape to that for F_1 and F_2. We know from years of measurements of unpolarized scattering that F_1 and F_2 have significant Q^2 dependence. A recent analysis of SLAC electron and BCDMS muon data for F_2 by Virchaux and Milsztajn[19] is shown in Figure 1. Since the asymmetry $A_1 \simeq g_1/F_1 = g_1 2x(1+R)/F_2$, and if the Q^2 dependence of g_1, F_1, and F_2 comes only from QCD evolution, we would expect the A_1 asymmetry to be independendt of Q^2, and that would be the end of the story.

However, we also know from the Virchaux-Milsztajn analysis that F_2 has significant non-scaling contributions from higher twist. The dashed curve in Figure 1, containing only QCD plus kinematic target mass corrections, does not fit the data. They find the best fit, shown by the solid curve in Figure 1, when they fit the data

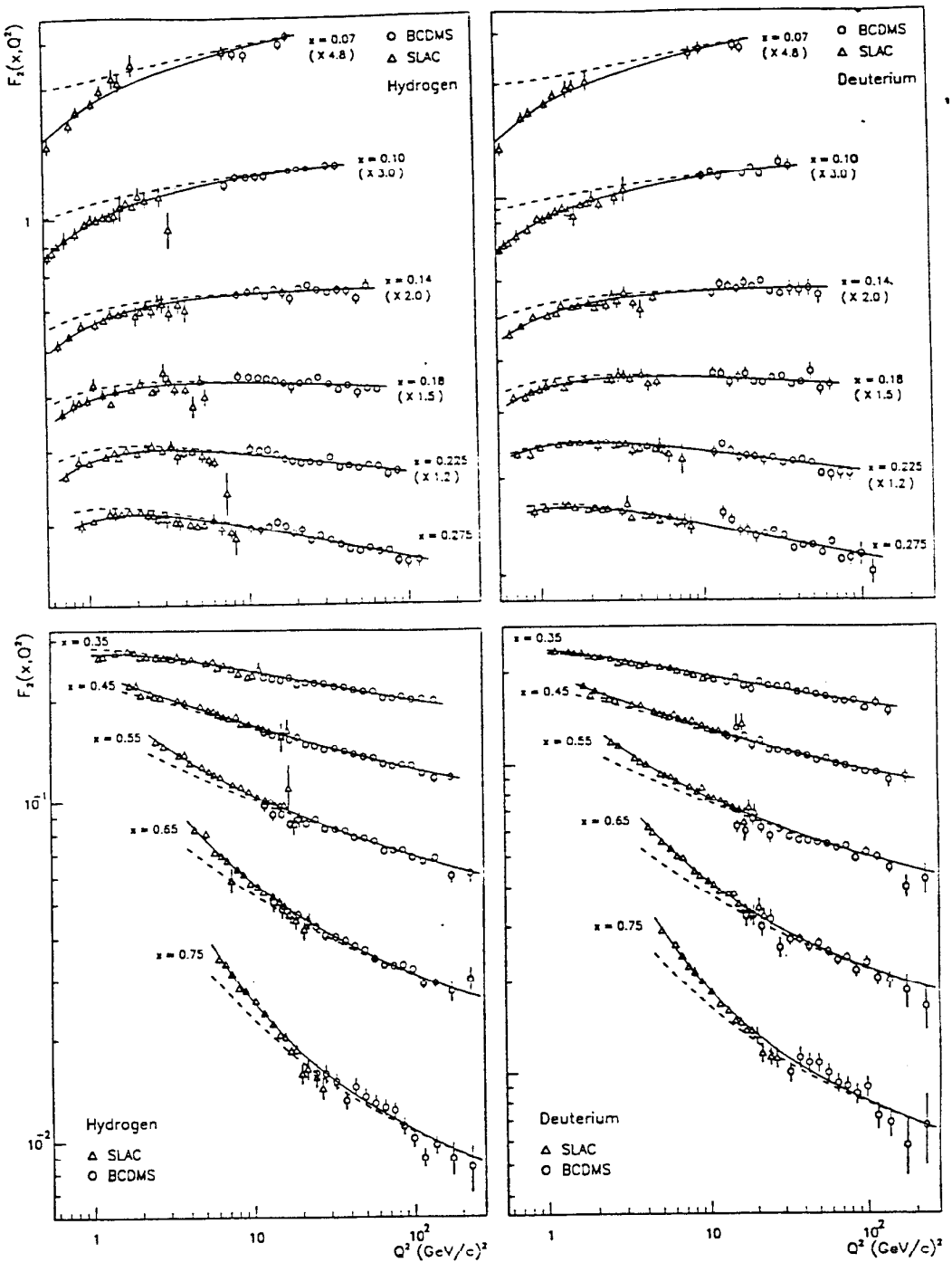

Fig 1. Next-to-leading order QCD fit to SLAC and BCDMS hydrogen and deuterium $F_2(x, Q^2)$ data with target mass corrections from Virchaux and Milsztajn [Ref (18)]. The solid line is the result of the full fit; the dashed line visualizes the Q^2 evolution without the twist-four corrections (leading-twist plus kinematic target mass corrections only).

to the form

$$F_2^{HT}(x_i, Q^2) = F_2^{LT}(x_i, Q^2)\left[1 + \frac{C_i^f}{Q^2}\right] \tag{11}$$

where the C_i^f coefficients parametrize the presence of twist-four terms that fall with $1/Q^2$. The C_i^f values from the fits, shown in Figure 2, correspond to twist-four contributions to F_2 as large as 15% to 20%.

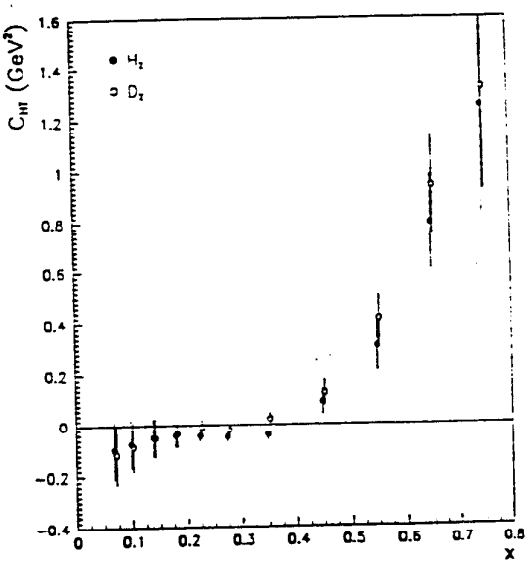

Fig. 2. The twist-four coefficients C_i^f as a function of x from Ref 19. Full (open) circles are for hydrogen (deuterium) data. The error in the C_i^f at low x is due to the uncertainty in the gluon structure function.

It is completely possible, even likely, that the spin structure functions, if examined closely enough, would also reveal non-scaling contributions at low Q^2. The origin of such terms, roughly speaking, corresponds to the virtual photon interacting with correlated quarks in the nucleon wave function (the diquark model is one extreme example). The scattering from such correlated quarks occurs with an extra penalty of $1/Q^2$ for finding the quarks in the correlated state. The spin structure functions of such correlations would not be the same as for single quarks. Two quarks can couple to either spin-zero or spin-one, which give different contributions to the $\sigma^{\uparrow\uparrow}$, $\sigma^{\uparrow\downarrow}$, $\sigma^{\uparrow\rightarrow}$ and $\sigma^{\uparrow\leftarrow}$. Therefore the spin structure functions

might also be approximated with the form

$$g_1^{HT}(x_i, Q^2) = g_1^{LT}(x_i, Q^2)\left[1 + \frac{C_i^g}{Q^2}\right]. \tag{12}$$

The coefficients C_i^g would not necessarily be the same as the C_i^f for the spin-averaged structure functions, and could possibly be larger. However, taking the result of the Virchaux-Milsztajn fits as a guide, there could be twist-four contributions to the g_1 on the order of 15% to 20% for Q^2 below 10 (Gev/c)^2. Therefore when, as we propose, the spin structure functions g_1^p and g_1^d are measured with an accuracy of 5% to 8%, and especially when the Q^2 is below 10 (GeV/c)^2, we must look for the non-scaling contributions that might interfere with our interpretation of the sum rules. If such non-scaling terms can be observed, this information would be an important addition to our picture of nucleon structure.

There is ongoing theoretical work[20,21] in calculation of higher twist contributions to the spin asymmetries. A recent analysis of the EMC and SLAC data by Ellis and Karliner[22] shows that higher twist corrections could be important for interpretation of the data to test the sum rules

If the higher-twist contributions are present and not accounted for, this would generate a systematic bias in the experimental test of the sum rules in experiments E142 and E143, which measure at $Q^2 < 10$ (GeV/c)^2. If the higher-twist contributions are as large as 10% to 15%, then lack of knowledge of the higher-twist corrections could be the largest source of systematic error.

III. SUMMARY AND COMPARISON OF PREVIOUS RESULTS

Measurements of the spin asymmetry, A_1^p, of the proton have been carried out at SLAC[7,8] and at CERN.[6] Future measurements are scheduled to be made at SLAC in experiment E143 and at CERN by the Spin Muon Collaboration (SMC),[3] and HERMES. Measurements of the neutron spin asymmetry, A_1^n, have been made by SLAC experiment E142[5] and measurements of the deuteron spin asymmetry,

A_1^d, have been made by the SMC.[4] CERN has an advantage over SLAC in being able to make the measurements at higher beam energy (E = 100 to 200 GeV) and thus measure at higher Q^2 on the average, and can reach lower x while keeping $Q^2 > 1$ (GeV/c)^2. However the available counting rates at CERN are low and the errors from EMC and SMC results have been dominated by statistical errors. SLAC has the advantage over CERN of being able to make the measurements with significantly smaller errors, primarily due to much higher counting rates, but also due to better precision in some important parameters (beam polarization, random helicity flips on every pulse to eliminate false asymmetries from long term changes in counting rates, measurements of $A^\perp$).

Following is a summary of the experimental sum rule results which have been extracted from the asymmetry measurements. EMC[6] found that $\int g_1^p dx = 0.125 \pm 0.010 \pm 0.015$ which is in disagreement with the expected Ellis-Jaffe result given in Eq. (10). The first error is statistical and the second is systematic. SMC[4] found $\int g_1^d dx = 0.046 \pm 0.040 \pm 0.030$ and, using the EMC results, that $\int g_1^n dx = -0.08 \pm 0.04 \pm 0.04$ and $\int (g_1^p - g_1^n) dx = 0.20 \pm 0.05 \pm 0.04$. [Note: we use $g_1^d = g_1^p + g_1^n$ rather than $g_1^d = (g_1^p - g_1^n)/2$ used by SMC.] These results agree within errors with both the Ellis-Jaffe and Bjorken sum rule expectations. E142[5] has found, $\int g_1^n dx = -0.022 \pm 0.006 \pm 0.009$. This result together with the integral over the proton $g_1^p(x)$ from EMC gives the integral $\int (g_1^p - g_1^n) dx = 0.148 \pm 0.012 \pm 0.018$. Using a revised[23] EMC value of $\int g_1^p dx = 0.135$ raises the value of the Bjorken integral to 0.158. This is to be compared to a Bjorken sum rule prediction of 0.180 ± 0.004, using $\alpha_s = 0.33 \pm 0.06$ for Q^2 between 2 and 10 (GeV/c)^2. The average Q^2 for the EMC data is 10.7 (GeV/c)^2, for the SMC data is 4.6 (GeV/c)^2, and for E142 is 2 (GeV/c)^2. The E142 and SMC results are consistent with each other within the errors (large for SMC).

The less than perfect agreement with the Bjorken sum rule is not good news for QCD. However, the disagreement is only about 1.5σ, which could well be a fluctuation, and the systematic errors may have been underestimated. Given these results it is important to establish by independent experiments if there is a problem

with the existing measurements, or if there are significant effects, such as from higher twist or nuclear dependence of the structure functions, that is interfering with the interpretation of the data. The E143 experiment and the present proposal will address these issues.

IV. EXPERIMENT GOALS AND POSSIBLE RESULTS

Experiment Strategy

The goal of this proposal is to make precision measurements of the proton and neutron spin structure functions over the extended kinematic range available using a 48.6 GeV beam. The method used in this experiment is a direct extension of that to be used by E143. The principle features are:

1. Measurements of $A^{\parallel}$ and $A^{\perp}$ and σ for both proton (NH_3) and deuteron (ND_3) targets will be made. Values for $g_1^p(x)$, $g_2^p(x)$, $g_1^n(x)$, and $g_2^n(x)$ will be extracted using Equations (7)and (8). The asymmetry $A^{\parallel}$ will be determined from the measured asymmetry $\Delta^{\parallel}$ defined in terms of the number of events N with a given orientation of the beam and target polarizations (parallel or opposite):

$$\Delta^{\parallel} = \frac{N^{\uparrow\downarrow} - N^{\uparrow\uparrow}}{N^{\uparrow\downarrow} + N^{\uparrow\uparrow}} = P_b P_t f (1 + C_{15}) A^{\parallel}, \qquad (13).$$

The statistical crror on $A^{\parallel}$ is given by

$$\Delta A^{\parallel} = \frac{1}{\sqrt{N}} \frac{1}{P_b P_t f (1 + C_{15})} \qquad (14)$$

where $N = N^{\uparrow\downarrow} + N^{\uparrow\uparrow}$ is the total number of counts. The quantity $A^{\perp}$ is given by a similar equation from measurements of the asymmetry $\Delta^{\perp}$ in terms of $N^{\uparrow\leftarrow}$ and $N^{\downarrow\leftarrow}$ with opposite transverse target polarizations. The cross sections σ will be determined from a combination of measurements in this experiment for $x < 0.1$, and from normalization to the precision cross sections from E140, E140x, and NMC for $x > 0.1$. The neutron asymmetries

are extracted from measurements on the deuteron using

$$A_n = \left(1 + \frac{\sigma_p}{\sigma_n}\right)\frac{A_d}{\gamma} - \left(\frac{\sigma_p}{\sigma_n}\right)A_p \tag{15}$$

where σ_p/σ_n is extracted from unpolarized deep inelastic scattering data on hydrogen and deuterium. The factor $\gamma \simeq 0.92$ is the effective polarization of the nucleons in the deuteron, discounting those in the D-state. These expressions depend on the polarization of the beam $P_b(\sim 0.8)$ and target free protons $P_t(\sim 0.9)$ and deuterons ($P_t \sim 0.4$) and on the dilution factor $f(\sim 0.12)$, which represents the ratio of the probability of scattering from free protons or deuterons to the probability of scattering from all the nucleons in the target. The correction term C_{15} includes the effects of the nitrogen polarization in the ammonia molecule, and is of the order of 1.5% in NH3 and 5% in ND3, and the errors are $\sim$ 10% of the correction.

2. The x and Q^2 range will be extended by using a 48.6 GeV beam and a system of spectrometers and detectors optimized for that energy.

3. The experimental errors will be reduced as far as practical. The spectrometer, detector, and data acquisition systems have been designed to maximize the counting rates as far as possible within the constraints from the expected backgrounds. We also plan to make many checks and auxiliary measurements to calibrate the system and measure systematic effects and backgrounds.

The optimization of the spectrometers and detectors to achieve these goals is described in the next section. The parameters and assumptions used in the estimates of counting rates and experimental errors are given in Appendix B. The run plan to achieve these goals is given in Table IV in the last section.

Possible Results

The possible results of this experiment and comparisons with other existing data are shown in Figures 3 through 8. The main results of this experiment will be:

1. Precision measurements would be extended down to x of 0.015 and up to x of 0.85. This will cut in half the region at low x where precision cross sections are unmeasured by E142/E143, giving a corresponding reduction in the uncertainty from extrapolation of the sum rule integrals to $x = 0$. The new data will significantly extend the range of precision measurements at high x and sharply reduce the error from extrapolation to $x = 1$.

2. The statistical errors on g_1^p will be a factor of 5 to 6 times smaller than those on the EMC measurements. The statistical errors on g_1^d will be a factor of 9 to 12 times smaller than those recently reported by SMC. The statistical errors on the extracted neutron g_1^n will be smaller by a factor of about 0.6 from those measured by E142.

3. For five or six x bins in the range $0.02 \leq x \leq 0.85$ there will be data of sufficient precision, together with data from E143 at lower Q^2, to measure the Q^2 dependence of A_1^p and A_1^d over roughly a factor of 2 to 3 range in Q^2 between $Q^2 = 1.5$ and 17 $(\mathrm{GeV/c})^2$. This is precisely the region where higher twist terms, if they exist, might be large enough to measure. Figure 8. shows expected errors attainable for a Q^2 dependent measurement of possible higher twist effects in the asymmetries for the proton and deuteron. To understand the relationship between the C_{HT} factors shown in these plots and those of the structure functions defined in Eqs. 10 and 11, we can write:

$$g_1^{LT}(1 + \frac{C_i^g}{Q^2}) = B_k A_1^{LT}(1 + \frac{C_{HT}}{Q^2}) F_2^{LT}(1 + \frac{C_i^f}{Q^2})$$

If we ignore the Q^2 dependence of the factor $R = \frac{\sigma_L}{\sigma_T}$ which is contained in the kinematic factor B_k then to a first approximation:

$$g_1^{LT}(1 + \frac{C_i^g}{Q^2}) \sim B_k A_1^{LT} F_2^{LT}(1 + \frac{C_{HT} + C_i^f}{Q^2} + O(\frac{1}{Q^4}))$$

which implies that $C_i^g \sim C_{HT} + C_i^f$.

4. Measurements of $A^{\perp}$ will reduce the error from its contribution to g_1 to negligible values. If g_2 turns out to be larger than some models suggest, but considerably smaller than the theoretical limit from $|A_2| \leq \sqrt{R}$, then it can be measured using $A^{\perp}$ and $A^{\parallel}$.

Table I gives a list of the sources and the expected values for the systematic errors of this experiment. Table II shows a comparison of estimates of the various sources of errors on the extracted integrals over the spin structure functions from the competing experiments.

The bottom line is that, barring large differences in the measured values of $g_1^p(x)$ and $g_1^n(x)$ from the ones assumed in these estimates, this experiment will reduce the errors on the sum rules from extrapolation of the integrals by roughly a factor of 2 in the Bjorken sum rule from the expected E143 results and test the Bjorken sum rule to the level of 1.6% statistical error and 6.4% systematic error. This is accomplished primarily by extending the measurements to lower and higher x, by reducing the statistical and systematic errors, by measuring the contribution from g_2, and by measuring or eliminating any contributions from higher-twist terms. These estimates assume that the functions are well behaved near $x = 0$. If nature turns out to have a different plan that gives some large excursions of the spin structure functions at low x, then precision measurements at the lowest possible x will be essential for making a reliable extrapolation.

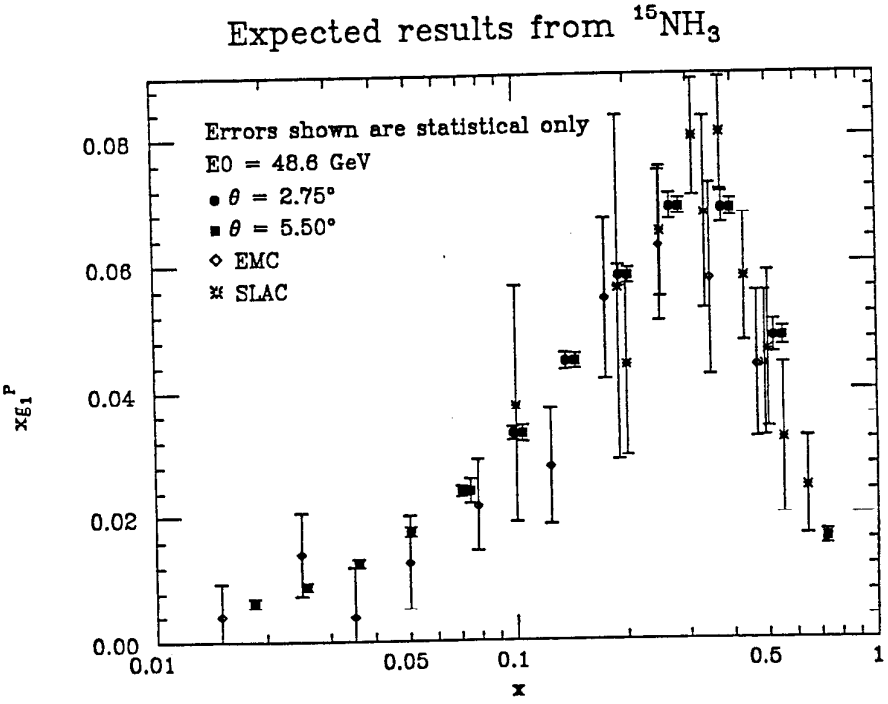

Fig. 3. Possible results for $xg_1^p(x)$ (statistical errors only) for possible data in the 2.75° and the 5.5° spectrometers. The previous data are from EMC (Ref. 6) and SLAC (Refs. 7, 8).

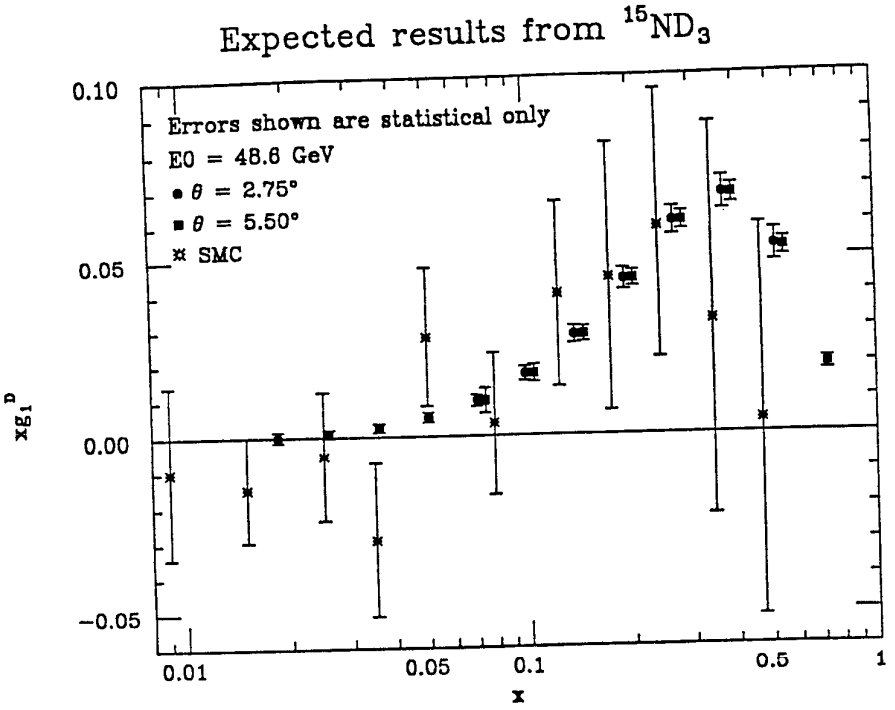

Fig. 4. Possible results for $xg_1^d(x)$ (statistical errors only). The values of xg_1^d shown assume the fit to A_1^p given in Appendix B that agrees with SLAC/EMC data and the fit to values of A_1^n from E142 shown in in Fig. 5 and also in Appendix B.

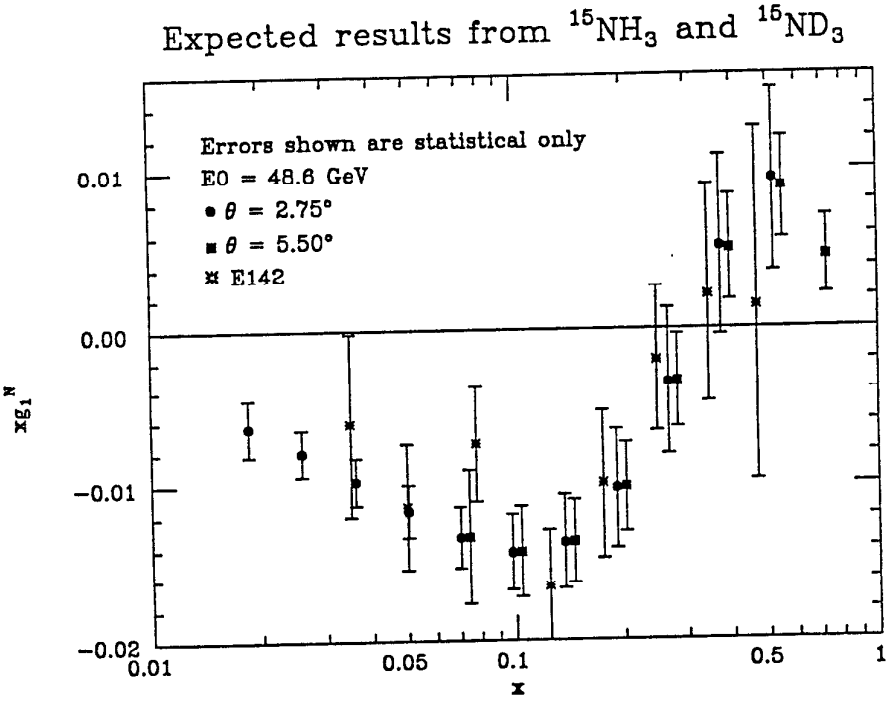

Fig. 5. Possible results for $xg_1^n(x)$ (statistical errors only) together with E142 data. The values for xg_1^n are from a fit to A_1^n from E142 data given in Appendix B.

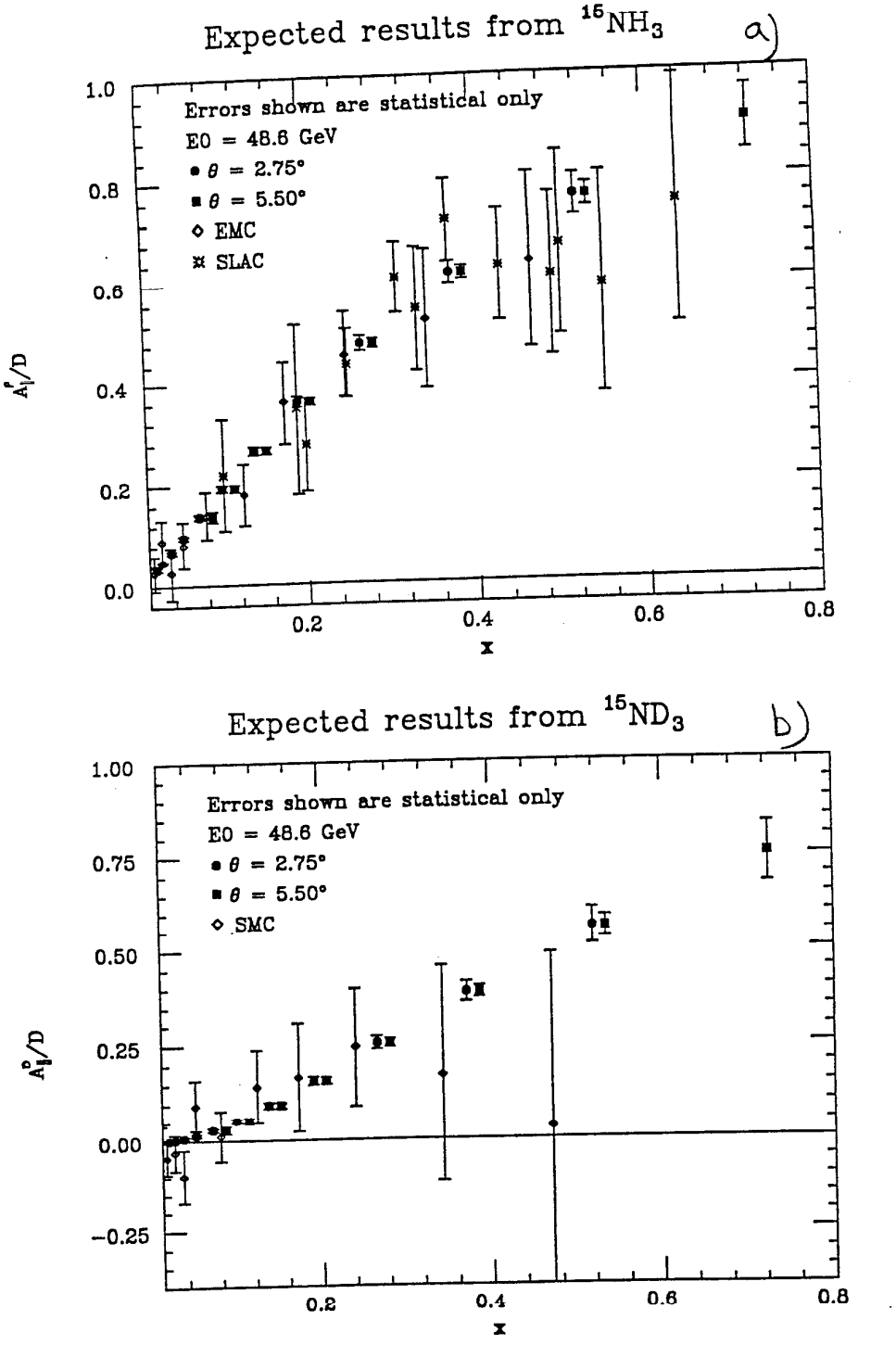

Fig. 6. Part a) possible results for $A_{\|}^p/D$ (statistical errors only) in the 2.75° and the 5.5° spectrometers. The previous data are from EMC (Ref. 6) and SLAC (Refs. 7, 8). b) possible results for $A_{\|}^d/D$ (statistical errors only). The values shown assume the fit to A_1^p given in Appendix B and the fit to values of A_1^n from E142 given in Appendix B.

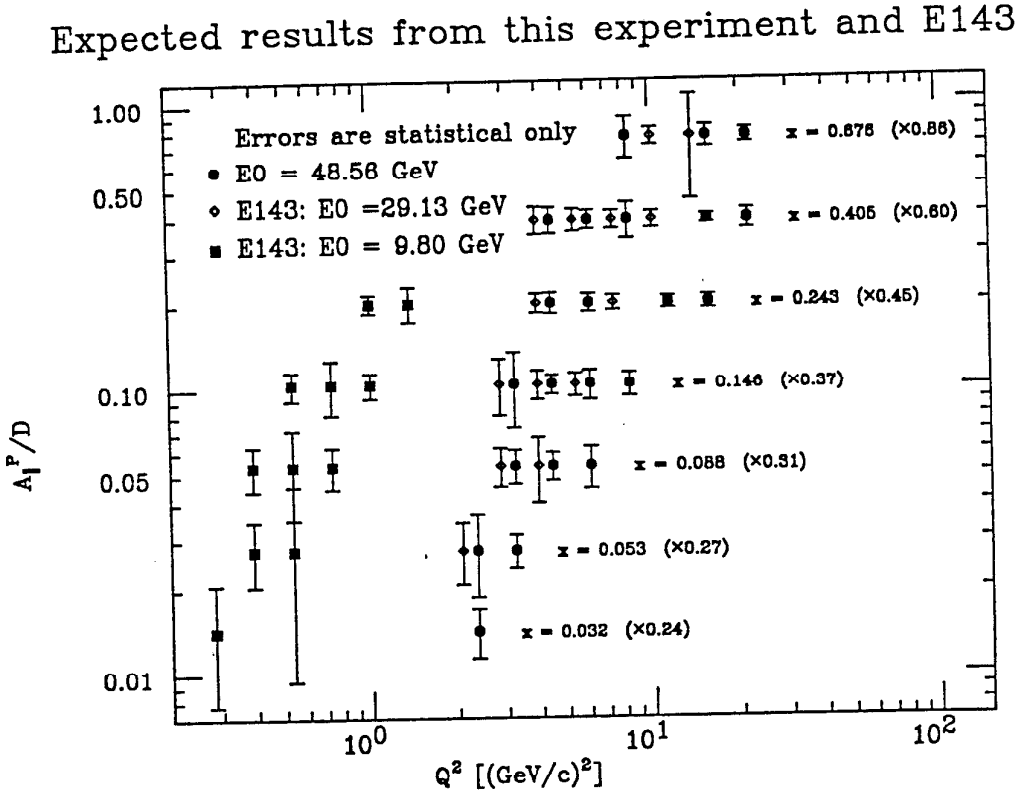

Fig. 7. Possible results for $A_{\parallel}^{p}/D$ combined with expected results from E143 at 9.3 GeV and 29.1 GeV. The combined data gives a larger range in Q^2 to look for higher twist contributions.

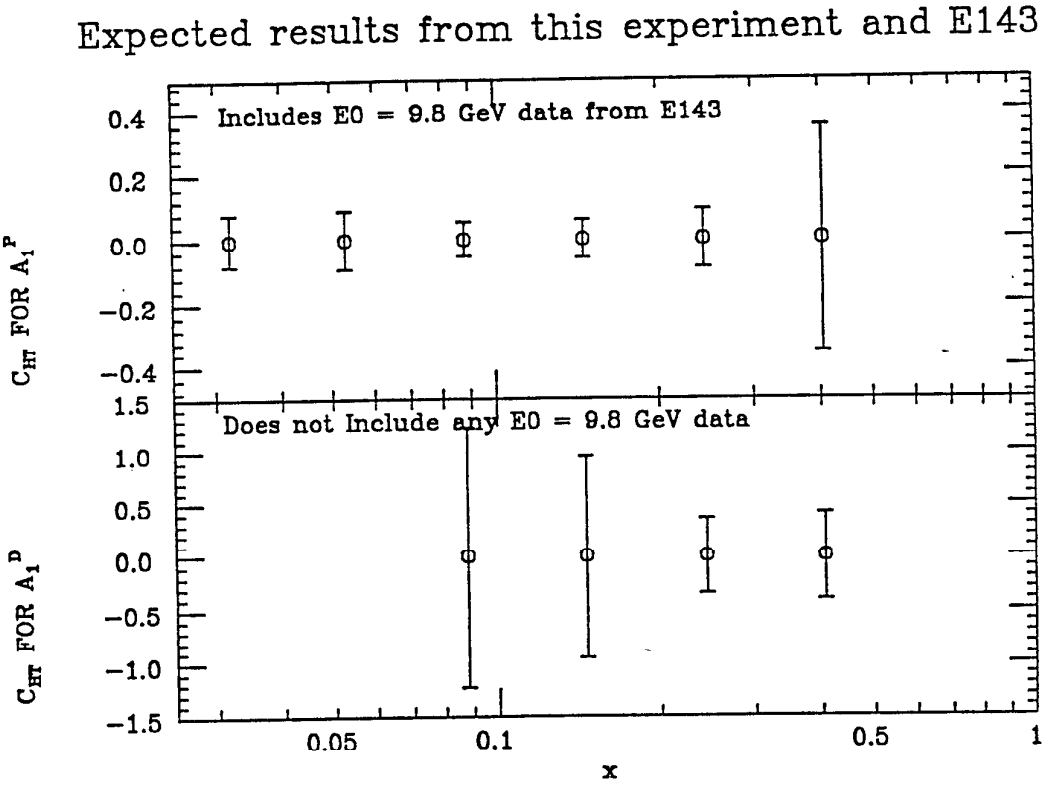

Fig. 8. Possible results for the coeficients $C_{HT}(x)$ for proton and deuteron that parametrize the possible higher twist terms in the asymmetries from the combined expected results from E143 at 9.8 and 29 GeV and this proposal at 49 GeV. The combined data gives a larger range in Q^2 to look for higher twist contributions.

Systematic Errors

In these estimates we have assumed that this experiment will be able to reduce some of the important systematic errors below the values assumed for E143. Partly this will be due to increased experience and understanding of our experimental equipment, and partly it will be due to the information gained in E143 that applies directly to some of the systematic uncertainties (measurements of the cross sections at low x and asymmetries at all x that are used in radiative corrections, for example). We will continue to work on reducing the systematic errors, and it is likely that experience with E143 will suggest a number of improvements to the techniques and operations that will reduce the errors further. An important result of the measurements versus Q^2 from this experiment and E143 is that we will be able to measure (or place limits on) the possible contributions from higher twist terms that could be contaminating the E143 (and E142) data. Contamination from higher twist, if it were present at the 10% to 15% level and not corrected, would be the largest source of systematic error.

The plan is to obtain g_1 and g_2 from the product of measured asymmetries and absolute cross sections (see Eq. 7 and 8). For $x > 0.07$ we will use a fit to world data, which is thought to be accurate to better than 2% for most of the x range. At lower x there is less data and the fit (mainly to NMC data) becomes less reliable. We plan to check the low-x extrapolation of the fit by making *relative* cross section measurements. We would determine an effective spectrometer acceptance at $x > 0.07$ where the world cross section is well known, and measure the cross section at lower x in the same acceptance region by lowering the field of the spectrometer in gradual steps. Uncertainties in the variation of radiative correction factors, pion and positron backgrounds, and possible rate effects will limit the accuracy of relative cross section measurements to about 3% except for the lowest x bin, where the uncertainty will be about 6%.

At high x there is a fairly strong sensitivity to the knowledge of the kinematic factors relating $A^{\parallel}$ and $A^{\perp}$ to g_1 and g_2. It terms out that the most important

sensitivity is to ν, which comes in linearly between $A^{\|}$ and g_1. Assuming we know E and E' to 1% leads to an uncertainty of about 3% in $\delta\nu/\nu$ in the highest x bins of each spectrometer. For $x < 0.5$, the uncertainty in the kinematic factors is generally $< 1\%$. This assumes that the average scattering angle in each kinematic bin is known to 0.5%, or 0.25 mr in the 2.75° spectrometer and 0.5 mr in the 5.5° spectrometer.

Uncertainties from the extrapolation to the unmeasured region near $x = 0$ and $x = 1$ are treated as systematic errors. Any extrapolation of the structure functions to the unmeasured regions is bound to be model dependent. The extrapolation error at low x is conservatively estimated based on a Regge parametrization ($g \sim x^{-\alpha}$) such that the estimate is maximized for reasonable choices of α. This error is strongly correlated with the errors (dominated by statistical errors) on $g_1(x)$ in the low x bins where the extrapolation begins. At high x the extrapolation error was also estimated, but the error is smaller than that for the low x extraplation because the highest x bin extends to $x = 0.85$.

Table I

Sources of Systematic Error

Source	Factor	$x-$Range	Error	Error on g_1^p	Error on g_1^d
x-dependent errors					
Cross section	σ	$x < 0.06$	3%	3%	3%
		$x > 0.06$	2%	2%	2%
Kinematic factor	$\delta\nu/\nu$	$x < 0.5$	1%	1%	1%
		$x > 0.5$	3%	3%	3%
Dilution factor	f		2%	2%	2%
Nitrogen correction	C_{15}			0.1%	0.5%
Radiative correction	C_R	$x < 0.03$	5%	5%	5%
		$x > 0.03$	3%	3%	3%
		$x > 0.06$	1%	1%	1%
π, e^+ correction	C_π	$x < 0.03$	5%	5%	5%
		$x > 0.03$	2%	2%	2%
		$x > 0.06$	$< 1\%$	$< 1\%$	$< 1\%$
Total x-dependent errors		$x < 0.03$		8.0%	8.0%
		$x > 0.03$		5.2%	5.2%
		$x > 0.06$		3.1%	3.2%
		$x > 0.50$		4.2%	4.3%
x-independent errors					
Beam polarization	P_b			3%	3%
Target polarization	P_t			2%	5%
Beam charge	$\mathcal{Q}$			0.2%	0.2%
Deuteron S State	γ				1.8%
Dead time,efficiency	C_{dt}			$< 1\%$	$< 1\%$
Total x-independent errors				3.7%	6.2%

TABLE II

Comparison of Errors for the Competing Spin structure Function Experiments
Error entries in the error table are in the form
statistical(% of sum)
systematic (% of sum)
extrapolation(% of sum)

	Sum	EMC+ SLAC	SMC	E142	E143	This Proposal
x_{min}		.01	.006	.03	.03	.015
x_{max}		.70	.60	.60	.70	.85
$\langle Q^2 \rangle$		10	5	2	3	4
$\int g_1^p dx$	.135[a]	.010(7.4%) .015(11%) .002(1.5%			.0027(2.0%) .0100(7%) .0023(1.7%)	.0011(1%) .0077(6%) .0011(1%)
$\int g_1^d dx$	.110[b]		.040(87%)* .030(65%)* .010(21%)*		.0049(5%) .0110(10%) .0037(4%)	.0020(2%) .0077(7%) .0018(2%)
$\int g_1^n dx$	$-.022$[c]		.04(50%)** .04(50%)** ? ?	.006(27%) .009(41%) .007(38%)	.0056(25%) .0124(56%) .0044(20%)	.0023(10%) .0062(28%) .0021(10%)
$\int (g_1^p - g_1^n) dx$	.180[d]		.050(25%)*** .040(20%)*** ? ?	.012(6.6%) .018(10%) .007(3.8%)	.0073(4.0%) .0230(13%) .0059(3%)	.0030(1.6%) .0115(6.4%) .0028(1.6%)

Notes:

The errors for this proposal take into account that most of the errors on g_1^p and g_1^d are correlated, and assumes that the error from g_2^p and g_2^n is negligible. Note: we use the definition that $g^d = g^p + g^n$ (*not* the average of proton and neutron).

[a] this is the revised EMC+SLAC result.

[b] from revised EMC+SLAC proton and E142 neutron.

[c] this is the E142 result.

[d] BJ sum rule using $\alpha_s = 0.33$. Does not agree with EMC+SLAC+E142 data

* percent errors of the sum $\int g_1^d dx = 0.046$ from SMC.

** percent errors of the sum $\int g_1^n dx = -0.08$ from SMC.

*** percent errors of the sum $\int (g_1^p - g_1^n) dx = 0.20$ from SMC.

V. EXPERIMENTAL METHOD

Overview

The primary constraints which affected the experiment design were the following:

1. Kinematic coverage – We want to measure at the lowest x possible and still keep $Q^2 > 1$ (GeV/c)^2 to satisfy the requirement of being in the scaling region. We also want coverage in Q^2 over as large an x range as possible with reasonable counting rates to look for Q^2 dependence. To achieve both the x and Q^2 goals requires spectrometers at two different angles. With fixed beam energy, the $Q^2 > 1$ limit, together with the mechanical constraints from the sizes of magnets and the floor space in the End Station, determines the minimum usable scattering angle to be 2.75 degrees. At fixed beam energy it is primarily the decline in counting rate at large Q^2 and high x which determines the optimum large scattering angle to be 5.5 degrees. Coverage at the high x end is also improved by going to higher beam energy because the limit of $W > 2$ GeV required to stay out of the resonance region can be met at higher x. There will also be some coverage at high x where $W < 2$ in the resonance region that will be useful. The kinematic coverage of this proposal compared with that for E142 and expected for E143 are shown in Figure 9.

2. Pion background – The pion rates are large at low x which is low E'. The π/e rates for a few kinematic conditions at 49 GeV are shown in Figure 10. Since the π/e rates decrease at fixed x with decreasing scattering angle, it is best to run at the smallest practical angle.

3. Radiative corrections – The radiative corrections increase at low E'. In general, we want to keep the potential error from uncertainty in the radiative corrections from being much larger than the other systematic errors, which vary from about 3% to 8% and depend on x. In previous experiments (E140, E140x) we have found that errors for radiative corrections to the unpolarized

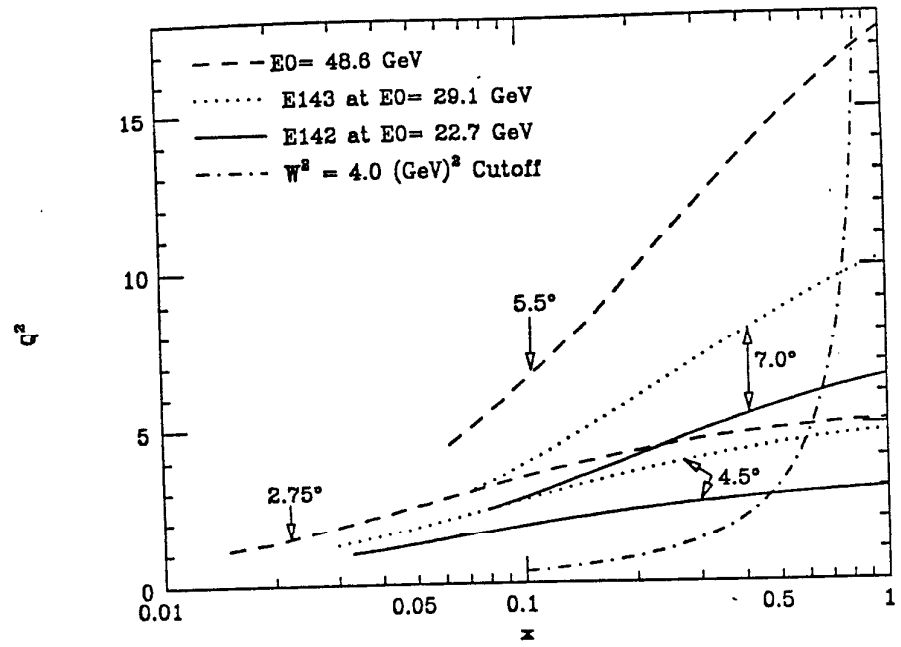

Fig. 9. The kinematic range in x and Q^2 of the proposed experiment, together with the range for E142 and projected for E143. The lines represent the center of the spectrometer acceptance at the indicated angles.

Fig. 10. The estimated π/electron rates at selected kinematics. The top figure shows the sharp rise in the pion rate at low x for fixed angle. The bottom figure shows the steep rise in π/e ratio with increased angle for a fixed low value of x.

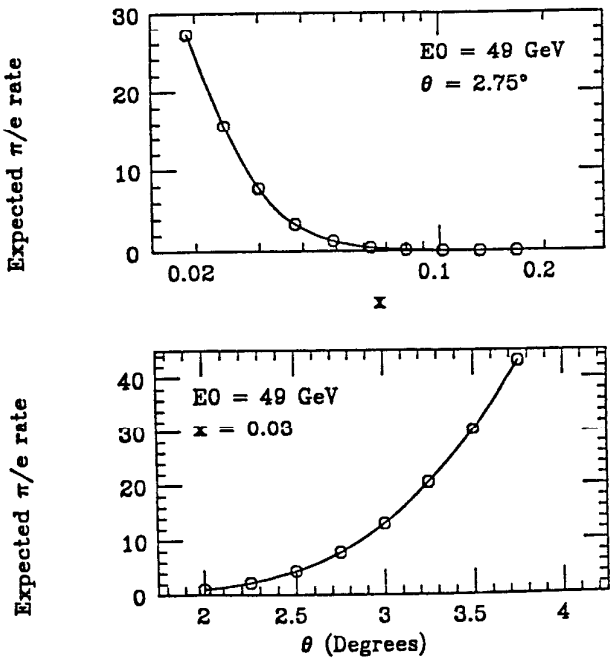

cross sections are about 1% as long as the corrections factors are ≤ 1.5. For the cross section measurements at low x the contributions from the elastic tail (known to 3% of its value) and inelastic tail (known to 3% of its value) are approximately equal to the Born cross sections. The α^4 and $\gamma - Z_0$ interference terms are less than 2%, and thus have small uncertainty. Therefore, the overall uncertainty to the extracted σ_{Born} due to radiative corrections in the lowest x bin is $\leq 5\%$. For the asymmetries, the uncertainty of the elastic form factors contributes an error of about 3%, and the error due to uncertainty on the inelastic is also about 3%. Thus the overall uncertainty in A_{Born} in the lowest x bin due to radiative corrections is about 5% of the value of the correction. The radiative corrections to the asymmetry are largest at small x ($A_{Born}/A_{Rad} \sim 0.4$ in the lowest x bin) and they decrease rapidly with increasing x.

4. Spectrometer and detector design summary – The key problem for the spectrometer design is to get large acceptance for 10 to 40 GeV scattered electrons while maintaining high rejection of the pion flux, remaining insensitive to low energy spray background, and achieving the resolution in angle and energy needed to measure x and Q^2 with reasonable accuracy. The scheme we propose is evolved from the style of spectrometers used for E142/E143. We propose to employ a shallow s-bend arrangement of dipoles for momentum dispersion and for bending away from direct view of the target. Quadrupoles are used for focussing and to deliver the particles into a region of space convenient for the detectors. Čerenkov detectors and lead glass shower counters will be used for electron identification, and scintillator hodoscopes for tracking. The magnets plus aperature defining masks will permit the scintillators and Čerenkov mirrors to be located in a region separated from direct view of the target by at least two bounces to minimize background from photons and neutrons. The focussing properties of the magnetic optics, together with the segmentation of the shower counters and the Čerenkov mirrors, is sufficient to measure the kinematics x and Q^2 of scattered electrons. Experience from

E142 shows that the Čerenkov and lead glass detectors will be relatively free of background from low energy photons and neutrons. If the background rates in the scintillators are also low enough to permit tracking of individual events, this will permit additional cuts for electron identification and help define the event kinematics (especially the vertical angle ϕ). If background rates in the scintillators prove to be too large for effective tracking, in this scheme the measurements can still be made using only the Čerenkov and lead glass detectors. The hodoscopes would be used for tracking at lower luminosity for system calibration.

In the following sections we describe the proposed experiment in more detail.

Beam

Beam energy – We propose to measure mostly at a beam energy of 48.55 GeV using the SLED beam with 120 ns pulse length. This is the highest energy for spin precession of $N\pi$ in the A-line that can be achieved leaving sufficient spare klystrons for reliable accelerator operation. To deliver beam energy higher than 29 GeV into End Station A requires more bending power in the A-line. This can be achieved by adding existing magnets to the bend string. A project for upgrading the A-line to 50 GeV is in progress. For a small fraction of the data we plan to run at a lower energy (perhaps 29 GeV) for normalization to measurements at the E143 kinematics.

Beam intensity – This experiment is limited to beam intensity around 2×10^9 electrons/pulse in a 120 ns SLED beam pulse to avoid heating and radiation damage to the polarized target. The actual beam intensities may be adjusted around this value for various tests and as experience establishes the actual limits of the target.

Polarization – For polarized beam we are assuming that beam with polarization of about 80% will be available from one of the strained lattice cathodes using the Ti-sapphire laser system now being tested for E143. The beam polarization will be flipped randomly on a pulse-to-pulse basis.

Beam rastering and control – Like E143, this experiment requires that the beam

be rastered over the front surface of the target material to spread out the heat and radiation damage over the full target volume. We will require that the beam rastering and control system, now being upgraded for E143, be capable of rastering the 50 GeV beam over a target roughly 2 cm in diameter.

Møller System

The beam polarization will be measured using single-arm and double-arm Møller scattering as in E143. It is possible that the Møller polarimeter will require little change for a beam energy of 50 GeV. The present Møller 18D72 spectrometer magnet will reach the momentum required to keep the Møller laboratory angle fixed to the nominal E142/E143 value of 7.77 mr. The Møller scatters then correspond to slightly backward hemisphere scattering at a CM angle of 120°, which is the kinematic condition used for the SLC Linac Møller polarimeter. The SLC Møller polarimeter has performed very well, and has comparable precision to the E142/E143 Møller polarimeter. There are advantages to running Møller scattering under these kinematic conditions. While the analyzing power is somewhat smaller than at CM angle of 90° for E142/E143, this disadvantage is more than offset by the reduced background from the radiative tail from nuclear elastic scattering.

Consequently at this time we see no problem adapting the E142/E143 Møller polarimeter for a 50 GeV beam. After experience with E143 and reconsideration of the optimum scattering momentum and angle, we may elect to adjust the Møller spectrometer by adding another magnet or modifying the layout in some way.

Beamline in End Station A

The measurement of the $A^{\perp}$ asymmetries requires that the 5 Tesla target field be oriented perpendicular to the beam direction. As in E143, to compensate for the vertical deflection of the beam, a four-magnet chicane will be used. The field in the chicane magnets is adjusted to give the same $\int Bdl$ in each magnet equal to half of that for the target. The chicane is only turned on when the $A^{\perp}$ measurements are being made and it remains fixed in field at all energies. The spectrometer plan described below uses the same upstream chicane system of 10D37 magnets as E143,

while the downstream 10D37 chicane magnet is slightly repositioned to avoid the spectrometer magnets.

The beamline down-stream of the target will be designed to gradually increase in diameter along its length to the back of the spectrometers, consistent with the constraints from the chicane and spectrometer magnets and shielding. The downstream beamline will contain some collimators and it will be closely integrated into the dense shielding between the spectrometers required to protect the detectors from target spray. As in E143 an SEM array will be used to measure beam profiles and the precision toroids will be used to measure beam currents.

Targets

The target for this proposal will be the same one used in E143. It consists of a five Tesla superconducting magnet, microwave systems for pumping the spins, NMR systems for measuring the polarization, and a cryostat and target refrigerator. This target uses irradiated frozen ammonia granules (NH_3) and deuterated (ND_3) cooled to $1K$. Under these conditions, ammonia has been shown[24][25] to have superior radiation resistance, allowing for high polarizations, luminosities of the order of $40 \times 10^{33}\text{cm}^{-2}\text{s}^{-1}$, and quick recovery of polarization losses. An open geometry superconducting Helmholtz coil provides the magnetic field to align the nuclei by the method of Dynamic Nuclear Polarization.

We expect the E143 systems will be useable without major changes, though experience may lead us to make some improvements. For the $A^{\|}$ and $A^{\perp}$ measurements we propose the target field will be oriented either parallel or perpendicular to the electron beam. The target stands, pipes, and other systems have been designed to allow a "quick" switch over by physically rotating the entire scattering chamber including the superconducting magnet in about one day.

We expect to achieve target polarizations greater than 90% for protons and 40% for deuterons. At repetition rates of 120 pulses per second, the heat deposition in the target limits the beam currents to about 2×10^9 electrons per linac pulse.

We note that the polarized target will be needed for the G_{En} experiment at

CEBAF, and that this experiment can only take place in a fairly narrow window of time (given by the availability of a high-polarization beam, but before the startup of multiuser operation). To the best of our knowledge this window will occur in the fall of 1995.

Since the target is a key feature of this experiment, we give here an extended description of the principles of its operation.

Solid polarized targets work on the principle of Dynamic Nuclear Polarization in which a target material, eg. butanol, ethylene glycol, or ammonia, is doped, by chemical or radiation techniques, with a dilute assembly of paramagnetic atoms. The material is cooled to $\leq$ 1K in a magnetic field of a few Tesla and then irradiated by microwaves to drive the hyperfine transition which allows the nucleon(ar) spins to be aligned. All elements present in the material which possess a magnetic moment can be polarized at the same time. For spin-1/2 the polarization P is given by:

$$P = \tanh[\mu B/kT_s]$$

where μ is the magnetic moment, B is the magnetic field, k is Boltzman's constant and T_s is the spin temperature.

For many particle scattering experiments, the choice of a polarized target is dictated by the requirement that a basic figure of merit, F, of the type

$$F = P^2 I$$

be as large as possible. Here P is the polarization and I is the beam intensity. For example in the case where I is limited for some reason the choice would likely lead to a dilution refrigerator. Operation at very low temperatures would mean proton polarizations of greater than 90%.

However for this experiment the beam intensities are such that the material must be very resistant to radiation damage and must operate in a cryogenic environment which allows the most efficient removal of heat deposited by the beam.

For these reasons the target material will be radiation-doped ammonia[26] (NH_3 and ND_3). The target system will be a ^{4}He evaporation refrigerator operating with a magnetic field of 5T. This is the same target to be used at SLAC for E143 during the Fall of 1993.

^{4}He is used because of its superior thermal properties compared to ^{3}He. Only 1K can be reached with ^{4}He so a 5T magnet is necessary to at least maintain the polarization which can be achieved by using ^{3}He at 0.5K in a field of 2.5T. Ammonia is the material of choice because of its resistance to radiation damage and its higher hydrogen or deuterium content compared to other materials.

Past experience at SLAC with a 5T/1K target[27] showed that operation with materials such as butanol doped with porphyrexide was limited by the radiation damage inflicted on the material. A large overhead in time was incurred because of the necessity to change the target at frequent intervals. Subsequently it was found, at Bonn,[28] at SLAC[24] and Michigan[29] under varying cryogenic conditions, that substantial polarizations could be obtained with radiation doped ammonia and that the radiation resistance was much better.

Development continued at Bonn, particularly with ND_3,[30] and at Michigan where it was found[25] that NH_3 could be quickly polarized to >90% in a 5T/1K system. At the AGS this target was used in a scattering experiment[31] using proton beams with intensities of up to 10^{11} protons/sec. Results relevant to this experiment are:

Radiation damage: The e^{-1} value for the initial fall of polarization with beam dose is 4×10^{15} protons/cm^2, a factor of ten better than the best chemically doped material. This is in very good agreement with the data of Seely et al.[32] from an electron beam at SLAC, and Althoff et al[33] from an electron beam at Bonn. After about 10^{15} protons pass through the target the radiation damage rate slows down giving an e^{-1} value of 1.3×10^{16} protons/cm^2. This is also in good agreement with the electron data.[32,33] In addition ammonia can be repeatedly annealed without loss of polarization, in contrast to chemically doped materials which have to be

replaced after a few anneals.

Beam heating: With the ^{4}He cryostat used at the AGS a beam of 8×10^{10} protons/sec could be directed onto the target with a loss of only 2% in polarization. For a ^{3}He system a beam of 2×10^{10} protons/sec reduced the polarization by 15%.

Annealing: Generally the target was annealed when the polarization fell to about 80%. On the basis of the radiation damage values given in 1) a total of 3.25×10^{15} protons passes through the target while the polarization falls from 97% to 80%. For this proposal running at 2.5×10^{11} electrons/sec this would mean annealing every 3.5 to 4 hours.

Polarization: The polarization is relatively insensitive to the bulk temperature. Even at 1.6K values of >70% were reached in 20 minutes.

Overall, an improvement of a factor of 12 in the figure of merit F, was achieved at the AGS by using this 5T/1K ^{4}He instead of the older 2.5T/0.5K ^{3}He target. There was also an increase in the operational efficiency. In comparison with the SLAC 5T/1K target used in previous experiments, with butanol as the target material, an increase in F of a factor of 10 should be obtained. We can also expect an increase in operational efficiency.

The radiation properties of ND_3 have been studied extensively by the Bonn group. Deuteron polarizations of about 50% have been obtained at 3.5T/0.3K with corresponding proton polarizations of about 100%. With additional 'in-situ' irradiation with the beam, a deuteron polarization of 40% is expected.

The disadvantage of using ammonia as a target is that the nitrogen is also polarized (up to about 20%). In the case of ^{14}N (spin 1) both the unpaired neutron and proton are polarized. But for ^{15}N (spin 1/2) there is only an unpaired proton to carry the polarization. The use of $^{15}ND_3$ and $^{15}NH_3$ as targets has several advantages the most important being a reduction in the systematic errors on the both the neutron and proton spin structure asymmetries. ^{15}N is commercially available at reasonable cost.

Spectrometers

The general layout of the proposed spectrometer and detector systems are shown in Figure 11. The spectrometer design is based closely on the design for E142/E143 in which two large dipole magnets are used in an S-bend configuration to achieve both a large momentum acceptance and a two-bounce geometry for the detectors. Two-bounce geometry means that neutral particles from the target (such as neutrons or soft photons) need to bounce off at least two surfaces to impinge on an element of the tracking system. Experience in E142, in which part of the 7° spectrometer was in the one-bounce region, shows that hodoscope fingers are two orders of magnitude noisier in the one-bounce region than in the two-bounce region.

The design for the 5.5° spectrometer is shown in Figure 13. The trajectories of particles in the vertical (bend) plane are shown in the top panel, while the lower panel shows the horizontal plane. The design is similar to the existing 4.5° spectrometer (which uses B204 and B82), expect that the front dipole is now B201 instead of B204, and a second quadrupole has been added after B82. B201 has an asymmetric coil and so can be placed closer to the beamline and to the target, allowing for a larger solid angle by more than a factor of two. Increased solid angle is also achieved by removing the vacuum chambers from all the magnets. The larger solid angle is needed because the electron rates are much lower at E=48.5 GeV than at E=22.7 GeV, and counting rate is crucial to achieving reasonable errors at high x. The second quadrupole is added to provide more of a momentum focus than is possible with a single quadrupole. The focus of low momentum particles is important in achieving good π/e separation, since for the lead glass detectors placed near the focus, the expected electron energy is known independent of tracking. This gives an extra layer of redundancy compared to a non-focusing system (such as the present 7° spectrometer). Another result of the quadrupoles is to disperse the rays in the horizontal dimension. Although more detector elements are required, the density of hits is reduced compared to having no quadrupole. This makes the problem of tracking with the short SLED pulse easier.

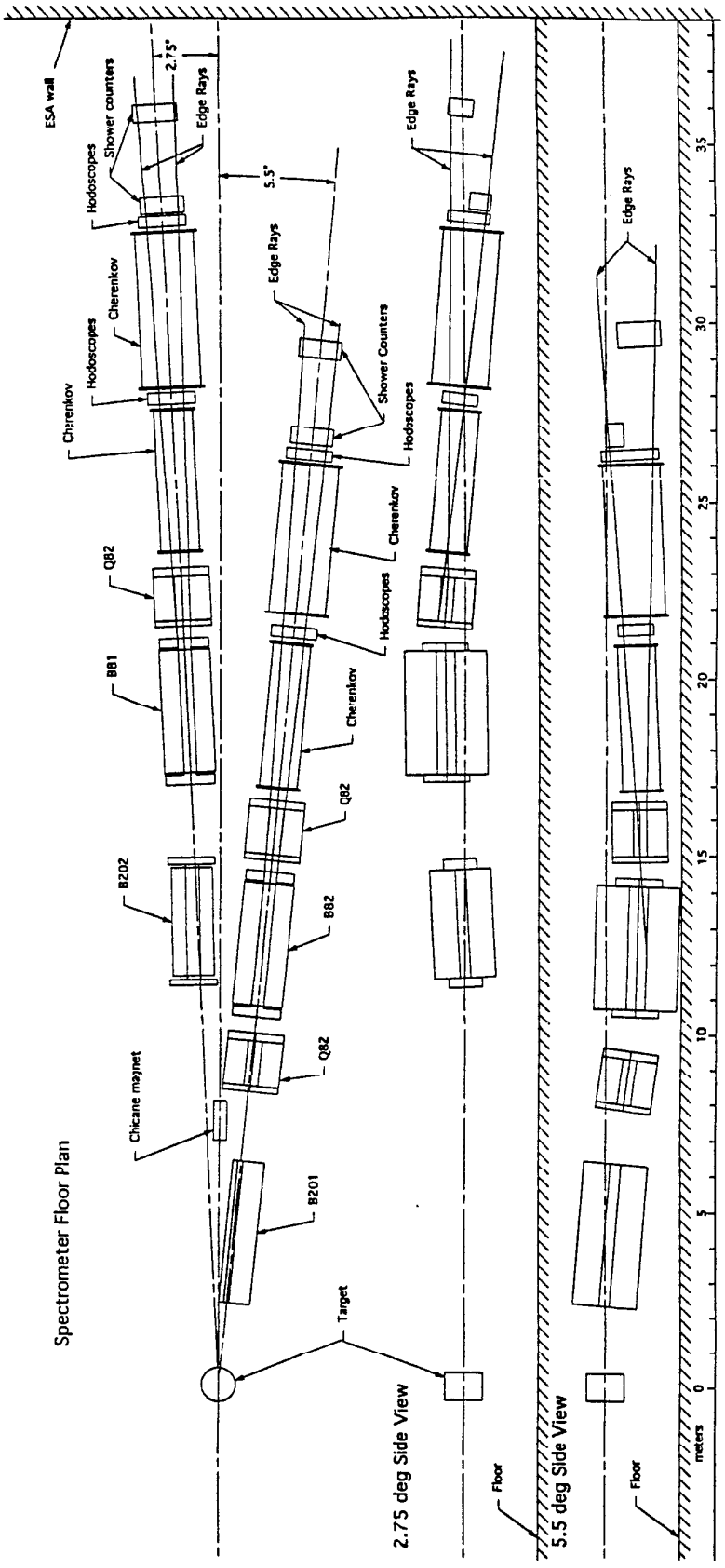

Fig. 11. Proposed spectrometer layout.

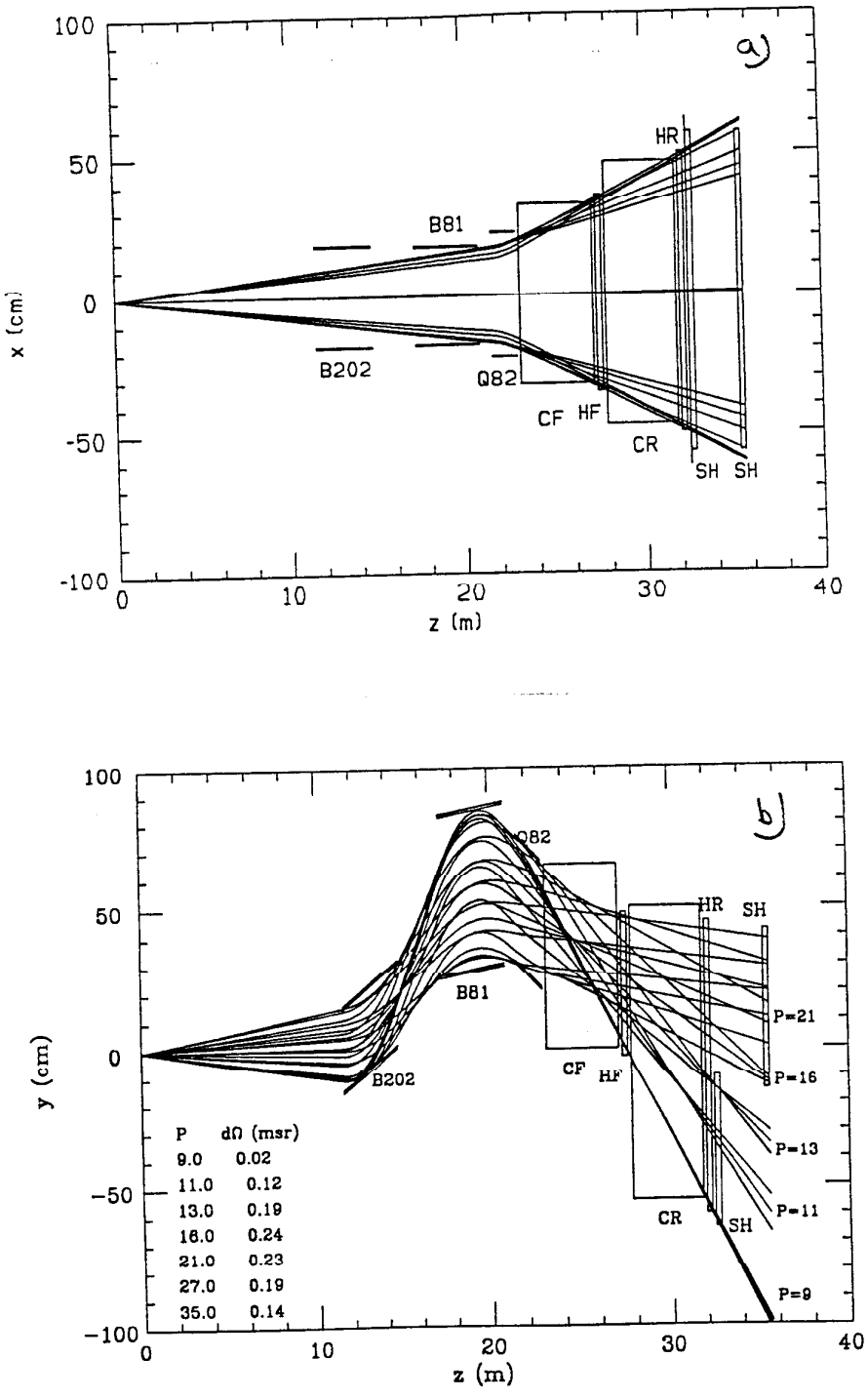

Fig. 12. The optics of the 2.75° spectrometer. Part a) in the non-bend plane, part b) in the bend plane.

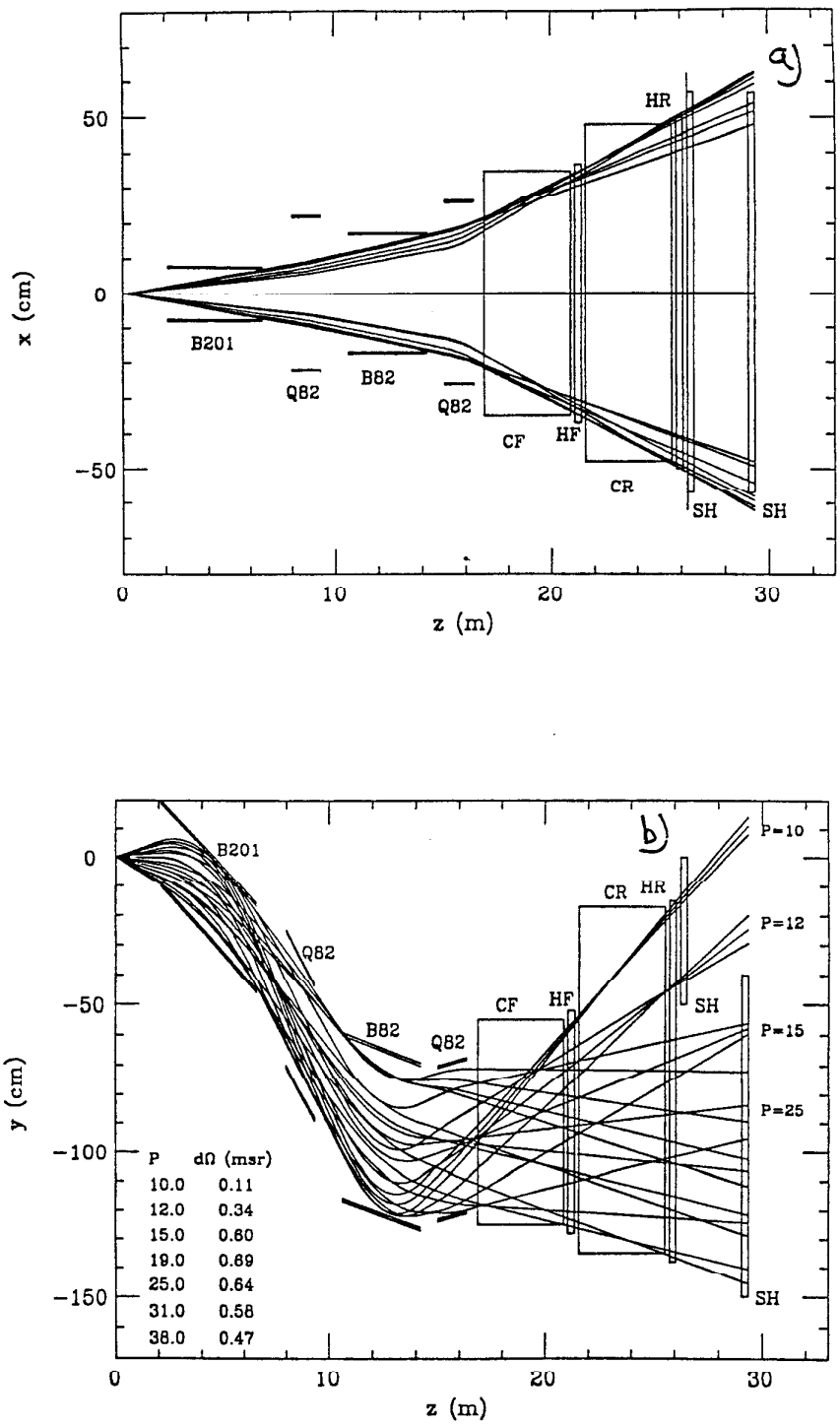

Fig 13. The optics of the 5.5° spectrometer. Part a) in the non-bend plane, part b) in the bend plane.

A variation on this design is also being considered, in which the quadrupoles would not be used, but a third dipole, bending in the horizontal plane, would be added. The dipoles in this case would be B201, B203, and B82. The advantage of this design is that the detectors would be further from the beam pipe, and the additional bending power would place them in a cleaner 2-bounce geometry. The increased length of the system would reduce the solid angle, and without quadrupoles we would have to rely on tracking to determine kinematics and separate pions from electrons.

The design for the 2.75° spectrometer, shown in Figure 12, is similar to the present 7° spectrometer. The same dipole magnets (B202 and B81) are used, but the distance from the target now has to be increased by about 6 m to accommodate the smaller scattering angle. The distance between the two magnets is also larger to preserve a two-bounce system for the higher range of E' that is required. As for the 5.5° spectrometer, a quadrupole has been added at the end to give a momentum focus for the lower momentum particles, where the pion contamination is the worst. The optics therefore allow an extra rejection power against pions in this crucial region. A three-dipole design (using B204, B202, and B81) is also being considered. The same trade-offs as for the 5.5° spectrometer apply.

The solid angle for the 2.75° and 5.5° spectrometers are plotted as a function of momentum in Figure 14. It can be seen that proposed spectrometers have about the same solid angle as the present 7° and 4.5° spectrometers, but are shifted to a higher momentum range to match the kinematic requirements of running at 48.5 GeV, and the central scattering angles are smaller. The large solid angles are needed to obtain adequate statistics for the Q^2-dependence studies. The sharp cutoff for momenta below about 10 GeV is needed to avoid the region where π/e ratios become larger than about 50:1, and where radiative corrections become prohibitively large. The horizontal acceptance of both spectrometers is relatively large: ± 8 mr for the 2.75° spectrometer, and from ± 7 mr to ± 11 mr for the 5.5° spectrometer (the range increasing with momentum). This allows study of Q^2-dependance of asymmetries both by comparing the two spectrometers where

they overlap kinematically, and also within the acceptance of each spectrometer individually.

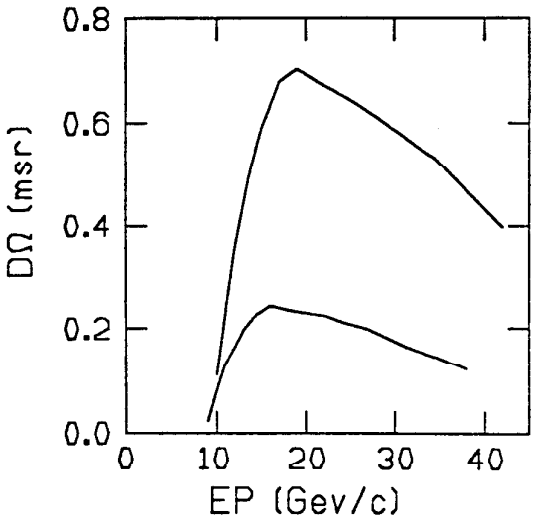

Fig. 14. The acceptance of the two spectrometers as a function of momentum.

Detectors

The detector design is based on a combination of elements that has worked well in most previous electron scattering experiments, including E142/E143. Pion/electron separation is one of the most crucial tasks for the detectors, especially since the π/e ratios will be up to five times higher than in E142. Pion rejection is achieved by two types of detectors: gas threshold Čerenkov counters which fire on all electrons, but only pions above a certain momentum threshold; and lead glass total absorption electromagnetic shower counters in which electrons deposit all of their energy, but pions only deposit a small portion, on average. Use of the shower counter requires knowing the momentum of the candidate particle in order to see if it matches the energy deposited (this is known as the E/P cut). This will be done in two ways: first from the optics that gives a momentum focus for the lower half of the momentum range, so that each block in the low momentum region has a narrow range of momenta that are optically allowed to contribute; second with tracking, if bacground rates in the scintillators are low enough, in which the momentum is determined by 'swimming' backwards through the magnets;

A second requirement of the detector system is to have sufficient momentum and scattering angle resolution to bin the data into bins of Q^2 and especially x

that are sufficiently small. The most stringent requirements are at high x, where a resolution of about $\pm 6\%$ in x is required to avoid mixing the resonance region counts ($W < 2$ GeV) into the highest x-bin of the deep-inelastic data. We also need to know the kinematic factors relating $A^{\parallel}$ and $A^{\perp}$ to g_1 and g_2 to 1%. This translates into a requirement of about $\pm 1.2\%$ momentum resolution for $P > 30$ GeV/c, and an angular resolution of ± 0.5 mr in the 5.5° spectrometer, and ± 0.25 mr in the 2.75° spectrometer. We propose to achieve the required momentum resolution primarily by upgrading the present lead glass blocks in the high momentum region from F2 to SF6 type glass, which has a resolution of better than $5\%/\sqrt{P}$. The required angular resolution is achieved in two ways: first by segmenting the shower counter array horizontally into at least 10 columns; second with tracking, if background rates in the scintillators are low enough. Both methods have been found to work well in E142.

Table III

Detector dimensions (x by y) for the proposed 2.75° and 5.5° spectrometers. Also listed are the dimensions of existing counters.

System	2.75°	5.5°	Existing 4.5°+7°
Front Čerenkov	64 by 65 cm^2	70 by 70 cm^2	
Rear Čerenkov	94 by 105 cm^2	95 by 112 cm^2	
Front Hodoscope	70 by 50 cm^2	75 by 75 cm^2	43 by (59 +69) cm^2
Rear Hodoscope	100 by 105 cm^2	100 by 115 cm^2	107 by (51+51) cm^2
Front Shower Counter	115 by 55 cm^2	115 by 50 cm^2	130 by (65+65) cm^2
Rear Shower Counter	115 by 68 cm^2	115 by 90 cm^2	

A listing of the approximate dimensions of the detectors needed for each spectrometer is given in Table III. The hodoscopes and shower counters cover a larger

surface area than in E142/E143, so additional detector elements will be required. The detector dimensions are given for the 2-dipole spectrometer designs, but similar sizes would be needed for the 3-dipole spectrometer designs. A more detailed discussion of each subsystem is given below.

Čerenkov Counters

We propose to use two 4 m long gas Čerenkov counters in each spectrometer. The particle envelopes are small enough to fit into the existing tanks, but the mirrors would have to cover a larger area, and for the 2.75° spectrometer would need to be segmented into two or preferably four segments to help reduce pile-up and accidental coincidences, which will be much more likely with the 100 nsec SLED beam pulse than with the 1-2 μsec non-SLED beam of E142/E143. The segmentation would reduce the average rate of electrons per mirror to 0.5/pulse. The back counter in each case could be made from the existing tanks, while for the front counters we would extend the existing 2 m tanks by an additional 2 m. While a portion of the front counters would then be in the one-bounce region, experience in E142 and also in the 1.6 GeV/c and 8 GeV/c spectrometers has shown that this does not seem to be a problem, since Čerenkov counters are quite insensitive to neutrons and low energy photons. In E142, the front and back Čerenkov counters counted at almost identical rates, even through the front counter was in the one-bounce region and the back one was not. In any case, the mirrors and phototubes would be out of the one-bounce region. In both counters the gas pressure would be adjusted to give a pion threshold of about 19 GeV/c. This will reduce the number of photoelectrons to about 3.3 per detector. Adding the two counters together will give about 7 photoelectrons, which gives an efficiency of 98% if a minimum of 2 photoelectrons are required. We can also reduce noise and accidentals, if necessary, by requiring at least one photoelectron in each counter, for a lowered efficiency of 92%. The expected rejection power against pions is estimated to be better than 1/20, mainly limited by accidental hits and pile-up effects with the short beam pulse. We plan to use flash ADC's on each Čerenkov phototube to reduce pile-up effects as much as possible.

Hodoscopes

In the present E142/E143 setup there are six planes of hodoscopes in each spectrometer. For the new spectrometers, we need to cover approximately twice the area. Since the expected real particle rates will be lower in the 5.5° spectrometer, it is reasonable to take all the approximately 400 existing hodoscope elements and combine them together to form the 5.5° spectrometer hodoscope planes. This will require some modifications of the support structures, and some longitudinal staggering so that the phototubes do not bump into each other, but otherwise is straightforward. For the higher rate 2.75° spectrometer, we propose to build a new set of finer-grained hodoscopes. As in our previous designs, there would be x, y, and u planes in both the front and rear locations. There would be about 250 front hodoscope elements, with typical finger widths of 1.5 cm, and about 250 rear hodoscope elements, with finger widths of about 1.7 cm. The phototubes could primarily be of the small, inexpensive type used in E142/E143. Each finger would go to a discriminator, and thence to a multi-hit TDC. This will require approximately doubling the number of existing discriminators and TDC's.

Shower Counters

As can be seen in Figures 12 and 13, the shower counters are at the rear of the detector package. Rather than making a single lead glass wall, we are studying the possibility of having two walls, the first one (close to the last Čerenkov) to be close to the focus for the lowest momentum particles, the second further back to be closer to the focus for intermediate momentum particles. Making a single wall at an intermediate z position would reduce the complication the for some particles, the back wall would see spray from the front wall, but the E' cut from momentum focus would be compromised. In either case, the area needed to be covered is about the same: 1.4 m^2 for the 2.75° spectrometer, and 1.6 m^2 for the 5.5° spectrometer.

The shower counter in E142/E143 consists of 400 lead glass blocks (200 per spectrometer) with an effective area of 6.5 cm^2, for a total coverage of 1.7 m^2. As can be seen from Table III, we need to cover a total area of 3.1 m^2, so at least 1.4

m^2 of additional lead glass will be needed. We propose to acquire SF6 lead glass blocks awith fron surface area of about 9 cm by 9 cm and use about 2/3 of them to covcr the high momentum region of the 5.5° spectrometer where momentum resolution is most important. The remaining 1/3 of them would be put in the regions with the worst π/e rates. The new SF6 glass will have more than a factor of two better resolution than the present F2-type blocks, and will also have better π/e separation since the number of interaction lengths per radiation length is much less in SF6 than in F2. A total of approximately 180 new blocks, each with high quality photomultiplier tubes, will be needed.

The PMTs on the existing F2 detectors have a gain and time response that is marginally adequate for E142/E143, and will result in even worse performance for the short pulse length and higher electron energy of the SLED beam. The biggest problem is that the tubes begin to saturate at relatively low voltages, resulting in signals that are small compared to the maximum range of the ADC's we are using. We are investigating whether new phototubes are needed, or if a new tube base design for the existing tubes could result in acceptable performance.

The SLED pulse is short enough that it is not worth making event triggers and trying to read the pulse height of a given shower block in time intervals shorter than the beam pulse. Therefore every block will go to an ADC whose gate is the beam pulse. In order to resolve overlapping electrons and pions, we will also use a TDC on each block. The TDCs will also be used to look for coincidences with the Čerenkov signals and with elements of the tracking system. This will require an increase in the mumber of TDC's from the present system, which has only one TDC per four blocks.

As an alternative or in addition to using TDC's on each lead glass block, we are investigating the usefulness of using Flash ADC's on each lead glass block. These would give a complete time picture of the event, and help considerably in separating overlapping pion and electrons. One possibility is to use an existing system from Mark II.[34] This FASTBUS system has 6 bit resolution and runs at

140 MHz. Other systems are also being investigated. If a Flash ADC system is used, a substantial upgrade in computing would be required.

Electronics and Data Acquisition

Since there are no longer special triggers for electrons and pions, the trigger electronics will be much simpler than for E142/E143. For every beam spill, the ADC gates for the lead glass blocks and Cerenkov counter will be opened, and a start given to the TDC's. We will have approximately three times as many TDC's as in the present setup, and the number of hits per channel is expected to approximately the same, so we will need to enhance our data taking capability by roughly a factor of two. The number of ADC's will be half of the present system (which allows up to four triggers per pulse), but the probability of an ADC to be above threshold will be higher, resulting in approximately the same data rate from ADC's as in the present system. If Flash ADC's are used on the lead glass blocks, another factor of two in data rate is expected.

IV. RUNPLAN AND REQUEST TO THE LABORATORY

Table IV
Run Plan and Beam Time Request

Data		Hours
NH3 Parallel		180
ND3 Parallel		300
NH3 Perpendicular		45
ND3 Perpendicular		70
Calibration and normalization to E143		30
σ at low x		40
Positron and empty target		25
Empty target		40
Total hours at 100% efficiency		730
Overhead (target anealing, beam polarization measurements, target spin rotatations)	(×2)	1460
Laboratory efficiency	(×1.5)	2190
Total beam time request		13 calendar weeks

APPENDIX A

Kinematics and Structure Function Formulas

The experimental quantities used to determine the spin structure functions are the two asymmetries:

$$A^{\parallel} = \frac{\sigma^{\uparrow\downarrow} - \sigma^{\uparrow\uparrow}}{\sigma^{\uparrow\downarrow} + \sigma^{\uparrow\uparrow}} \quad \text{and} \quad \mathrm{A}^{\perp} = \frac{\sigma^{\downarrow\leftarrow} - \sigma^{\uparrow\leftarrow}}{\sigma^{\downarrow\leftarrow} + \sigma^{\uparrow\leftarrow}}. \tag{16}$$

Here $\sigma^{\uparrow\downarrow}(\sigma^{\uparrow\uparrow})$ is defined in Eq. (2), and $\sigma^{\downarrow\leftarrow}(\sigma^{\uparrow\leftarrow})$ is defined in Eq. (3). The experimental asymmetries $A^{\parallel}$ and $A^{\perp}$ are related to the virtual photon-nucleon longitudinal and transverse asymmetries A_1 and A_2,

$$A_1 = \frac{\sigma_{1/2} - \sigma_{3/2}}{\sigma_{1/2} + \sigma_{3/2}}, \quad \text{and} \quad \mathrm{A}_2 = \frac{\sigma_{\mathrm{TL}}}{\sigma_{\mathrm{T}}}.$$

$$A^{\parallel} = D(A_1 + \eta A_2) \ \text{ and } \ A^{\perp} = d(A_2 - \zeta A_1), \tag{17}$$

where

$$D = (1 - E'\epsilon/E)/(1 + \epsilon R), \tag{18}$$

$$\eta = (\epsilon\sqrt{Q^2}/(E - E'\epsilon), \tag{19}$$

$$d = D\sqrt{(2\epsilon/(1+\epsilon)}, \tag{20}$$

$$\zeta = \eta((1+\epsilon)/2\epsilon), \tag{21}$$

$$1/\epsilon = 1 + 2[1 + (\nu^2/Q^2)]\tan^2(\theta/2). \tag{22}$$

Here $\sigma_{1/2}(\sigma_{3/2})$ is the virtual photoabsorption cross section when the projection of the total angular momentum of the photon-nucleon system along the incident

lepton direction is $\frac{1}{2}(\frac{3}{2})$, and $\sigma_T = \frac{1}{2}(\sigma_{1/2} + \sigma_{3/2})$ is the total transverse photoabosrption cross section, and σ_{TL} is a term arising from the interference between transverse and longitudinal amplitudes. The factor $R = \sigma_L/\sigma_T$ is the ratio of longitudinal to transverse virtual photoabsorption cross-sections. The factor D is the virtual photon depolarization.

The virtual photon asymmetries A_1 and A_2 can in turn be expressed in terms of the measured $A^{\parallel}$ and $A^{\perp}$ as

$$A_1 = \frac{A^{\parallel}}{D[1+\zeta\eta]} - \frac{\eta A^{\perp}}{d[1+\zeta\eta]} \tag{23}$$

$$A_2 = \frac{\zeta A^{\parallel}}{D[1+\zeta\eta]} + \frac{A^{\perp}}{d[1+\zeta\eta]} \tag{24}$$

The asymmetries A_1 and A_2 can also be expressed in terms of the structure functions g_1 and g_2 as

$$A_1 = (g_1 - \gamma^2 g_2)\frac{1}{F_1} \quad \text{and} \quad A_2 = \gamma(g_1 + g_2)\frac{1}{F_1}, \tag{25}$$

where $\gamma = \sqrt{Q^2}/\nu$ and F_1 is the spin independent structure function.

Solving Equation (25) for g_1 and g_2

$$g_1 = \frac{F_1[A_1 + \gamma A_2]}{1+\gamma^2} \quad \text{and} \quad g_2 = \frac{F_1[\frac{1}{\gamma}A_2 - A_1]}{1+\gamma^2}. \tag{26}$$

In previous work where transverse asymmetries were not measured it has been customary to ignore the term containing A_2. Since γ and η are small at sufficiently large Q^2 in the kinematic range of the experiments, the approximation is made that

$$A_1 \simeq A^{\parallel}/D, \tag{27}$$

and then

$$g_1 \simeq A_1 F_1 = A_1 F_2/2x(1+R). \tag{28}$$

where F_2 is the second spin independent structure function. This is the method

used by EMC and SMC.

When transverse asymmetries are measured but the cross section σ is not measured, then the A_2 terms are included, but the factor R in the virtual photon depolarization needed to extract A_1 and A_2 from the measured $A^{\parallel}$ and $A^{\perp}$ must be determined from cross sections measured in other experiments or from models. This was the method used by E142 where the neutron spin structure function was extracted via $g_1^n = (A_1^n F_1^n + \gamma A_2^n F_1^n)/(1+\gamma^2)$. Here F_1^n is the spin averaged structure function of the neutron.

The experimental method proposed in this experiment will measure $A^{\parallel}$ and $A^{\perp}$ and the unpolarized cross section σ. The spin structure functions g_1 and g_2 will then be extracted directly from the measured quantities using the expressions[11]

$$g_1(x) - k g_2(x) = 2KA^{\parallel}\sigma/\sigma_{Mott}, \tag{29}$$

$$g_1(x) + k' g_2(x) = 2K'A^{\perp}\sigma/\sigma_{Mott}, \tag{30}$$

where the Mott cross section is

$$\sigma_{Mott} = 4\alpha^2 E'^2 \cos^2(\theta/2)/Q^4, \tag{31}$$

and the kinematical factors are defined by

$$K = EE'\cos^2(\theta/2)/[2x(E+E'\cos\theta)] \quad \text{and} \quad k = 2xM/(E+E'\cos\theta). \tag{32}$$

$$K' = E\cos^2(\theta/2)/(2x\sin\theta) \quad \text{and} \quad k' = 2E/(E-E'). \tag{33}$$

APPENDIX B

Factors and Assumptions Used in Estimating Kinematics, Counting Rates, and Experimental Errors

Assumptions for calculations

1. Beam current = 2.0×10^9 electrons/pulse.
2. Beam polarization = 80%.
3. Target density (NH3) = 0.917 g/cm^3.
4. Target density (ND3) = 1.056 g/cm^3.
5. Helium density = 0.145 g/cm^3.
6. Target length = 3.0 cm.
7. % ammonia in target = 60.0%.
8. % helium in target = 40.0%.
9. Amount of additional helium = 0.4 cm
10. ^{15}NH3 proton polarization = 90%.
11. ^{15}ND3 deuterium polarization = 40%.
12. ^{15}NH3 mass = 18.024 g/mole.
13. ^{15}ND3 mass = 21.042 g/mole.
14. ^{4}He mass = 4.003 g/mole.
15. 180 hours of data at 100% efficiency for NH3.
16. 300 hours of data at 100% efficiency for ND3.
17. Spectrometer solid angles versus E' as shown in Figure 14.

Kinematics

1. Beam energy = 48.55 GeV.
2. Small angle spectrometer $\theta_1 = 2.75 \pm 0.46$ degrees.
3. Large angle spectrometer $\theta_2 = 5.5 \pm \Delta\theta$ degrees, where $\Delta\theta$ ranges from 0.40 to 0.63 degrees. The θ acceptances are used in the Q^2-dependence calculations.

Notes

1. Minimum x attainable was based on π/e cut at 40 and $Q^2 > 1.0$.
2. Maximum x attainable was based on missing mass requirement $W^2 > 4$ to stay away from the resonance region.
3. NMC models[35] were used for F_2 and R.
4. Assumed $g_2 = 0$.
5. Pion rates were calculated via the WISER code[36] using a total of 5% radiator thickness.
6. 1.5% correction for nitrogen polarization was applied.
7. For E143 comparisons:
   (a) Beam energy = 9.8 and 29.13 GeV.
   (b) Small angle spectrometer $\theta_1 = 4.5 \pm 0.26$ degrees.
   (c) Large angle spectrometer $\theta_2 = 7.0 \pm 0.69$ degrees.
8. The proton asymmetry model from EMC[6] is slightly modified by the factor 1.071 to account for the change in the EMC and SLAC results due to reanalysis, where the Bjorken sum rule result changes from 0.126 to 0.135.

$$A_1^p = 1.071\left[1.025x^{0.12}[1.0 - \exp^{-2.7x}]\right]$$

9. Neutron asymmetry model[37] used:

$$A_1^n = 3.599x^{1.4}(1.0 - x) + x(3.648x - 2.665)$$

Created at 08:01 on 1-OCT-93 by LMS

For NH3 and ND3 targets:

BEAM:	2.0E+09	electrons/spill
	80.0	% polarization
TARGET:	3.0	cm length
	0.917	g/cm3 15NH3 density at 1K
	1.056	g/cm3 15ND3 density at 1K
	0.145	g/cm3 4He density at 1K
	40.0	% Helium content
	60.0	% Ammonia content
	90.0	% NH3 polarization
	40.0	% ND3 polarization

For 3He target:

BEAM:	1.0E+11	electrons/spill
	80.0	% polarization
TARGET:	30.0	cm length
	35.0	% Target polarization
	2.6E+20	nuclei/cm3 3He density
	2.1E+18	nuclei/cm3 N2 density
	0.020	cm glass thickness
	2.520	g/cm3 glass density

Solid angle reduced by 2.0 for small angle spectrometer

In the following table(s):
E0 is the incident beam energy in GeV.
TH is the scattering angle in degrees.
SA is the solid angle in msr.
EP is the scattering momentum in GeV.
Q2 is the four-momentum transfer squared in (GeV/c)**2.
W is the missing mass in GeV.
X is the Bjorken scaling variable.
DEPOL is the depolarization factor.
RC is the applied rad. cor. factor which divides the born cross sections to give raw cross sections
PI/E is the expected pion/electron rate ratio.
E/SPILL is the total expected electron counting rate per spill for the given x bin.
F is the dilution factor.
ERROR is the error on the measured asymmetry/DEPOL for PROTON, DEUTERON, OR NEUTRON assuming 180. hours of running (NH3), 300. hours of running (ND3) and 300. hours of running (3HE).

E0= 48.56; TH= 2.75

						********** NH3 **********					********** ND3 **********					********** 3HE **********				
EP	Q2	W	X	DEPOL	SA	RC	PI/E	E/SPILL	F	ERROR	RC	PI/E	E/SPILL	F	ERROR	RC	PI/E	E/SPILL	F	ERROR
11.3	1.3	8.3	.018	0.78	.142	0.43	25.53	0.195	0.15	.0045	0.43	25.53	0.219	0.26	.0044	0.55	26.21	0.184	0.13	.0094
14.0	1.6	8.0	.024	0.72	.217	0.50	13.27	0.284	0.15	.0037	0.50	13.27	0.319	0.26	.0037	0.61	12.96	0.281	0.13	.0079
17.0	1.9	7.6	.032	0.65	.243	0.58	5.59	0.307	0.15	.0037	0.58	5.59	0.344	0.26	.0037	0.68	5.25	0.316	0.13	.0078
20.3	2.3	7.2	.043	0.57	.233	0.65	1.94	0.286	0.15	.0041	0.65	1.94	0.321	0.26	.0040	0.74	1.77	0.304	0.13	.0087
23.8	2.7	6.7	.057	0.49	.213	0.73	0.57	0.257	0.16	.0047	0.73	0.57	0.288	0.26	.0047	0.81	0.51	0.280	0.13	.0101
27.3	3.1	6.1	.077	0.42	.195	0.80	0.15	0.231	0.16	.0055	0.80	0.15	0.258	0.26	.0056	0.87	0.13	0.257	0.13	.0122
30.7	3.4	5.6	.102	0.35	.165	0.88	0.03	0.190	0.16	.0069	0.88	0.03	0.212	0.26	.0071	0.94	0.03	0.215	0.13	.0156
33.8	3.8	5.0	.137	0.29	.147	0.95	0.01	0.163	0.16	.0085	0.95	0.01	0.182	0.26	.0089	1.00	0.01	0.188	0.13	.0201
36.6	4.1	4.4	.182	0.23	.130	1.03	0.00	0.135	0.16	.0109	1.03	0.00	0.150	0.26	.0115	1.07	0.00	0.157	0.12	.0270
39.0	4.4	3.8	.244	0.19	.114	1.10	0.00	0.105	0.17	.0144	1.10	0.00	0.116	0.26	.0158	1.13	0.00	0.124	0.11	.0389
SPECTROMETER TOTAL							10.82	2.153				10.85	2.410				7.88	2.306		

E0= 48.56; TH= 5.50

						********** NH3 **********					********** ND3 **********					********** 3HE **********				
EP	Q2	W	X	DEPOL	SA	RC	PI/E	E/SPILL	F	ERROR	RC	PI/E	E/SPILL	F	ERROR	RC	PI/E	E/SPILL	F	ERROR
11.2	5.0	8.1	.071	0.81	.256	0.57	21.90	0.018	0.16	.0119	0.57	21.90	0.021	0.26	.0120	0.68	20.73	0.038	0.13	.0185
13.6	6.1	7.8	.092	0.78	.493	0.67	6.65	0.032	0.16	.0087	0.67	6.65	0.035	0.26	.0089	0.76	6.03	0.068	0.13	.0139
16.2	7.3	7.4	.120	0.73	.644	0.77	1.56	0.037	0.16	.0079	0.77	1.56	0.041	0.26	.0081	0.84	1.37	0.082	0.13	.0130
19.2	8.6	6.9	.156	0.67	.704	0.87	0.29	0.036	0.16	.0080	0.87	0.29	0.040	0.26	.0084	0.93	0.25	0.082	0.12	.0138
22.3	10.0	6.3	.202	0.61	.657	0.97	0.04	0.030	0.17	.0091	0.97	0.04	0.033	0.26	.0097	1.01	0.04	0.069	0.12	.0166
25.5	11.4	5.7	.263	0.54	.633	1.07	0.01	0.024	0.17	.0106	1.07	0.01	0.026	0.26	.0118	1.10	0.00	0.056	0.11	.0211
28.6	12.8	5.1	.341	0.46	.581	1.17	0.00	0.016	0.18	.0136	1.17	0.00	0.018	0.26	.0157	1.18	0.00	0.040	0.10	.0304
31.6	14.1	4.3	.443	0.39	.568	1.27	0.00	0.010	0.19	.0188	1.27	0.00	0.011	0.26	.0228	1.27	0.00	0.025	0.09	.0489
34.3	15.4	3.5	.575	0.32	.534	1.37	0.00	0.004	0.20	.0318	1.37	0.00	0.005	0.26	.0405	1.35	0.00	0.011	0.08	.0975
36.8	16.5	2.5	.747	0.26	.490	1.47	0.00	0.001	0.20	.0799	1.47	0.00	0.001	0.26	.1022	1.43	0.00	0.002	0.08	.2491
SPECTROMETER TOTAL							5.31	0.209				5.36	0.231				3.92	0.473		

APPENDIX C

POSSIBLE RESULTS WITH A He TARGET

The spectrometer and detector systems outlined in this proposal would be capable of making measurements under the conditions required for use with a polarized ^{3}He target like the one used in E142. In that case since the target densities are much smaller than for the ammonia targets, the beam currents could be increased probably up to the maximum that could be delivered with the SLED beam. This would result in luminositics and counting rates in the spectrometers similar to those for the ammonia targets. In the following figures we show the possible results for measurements of the neutron spin structure using this system and with target parameters as for E142.

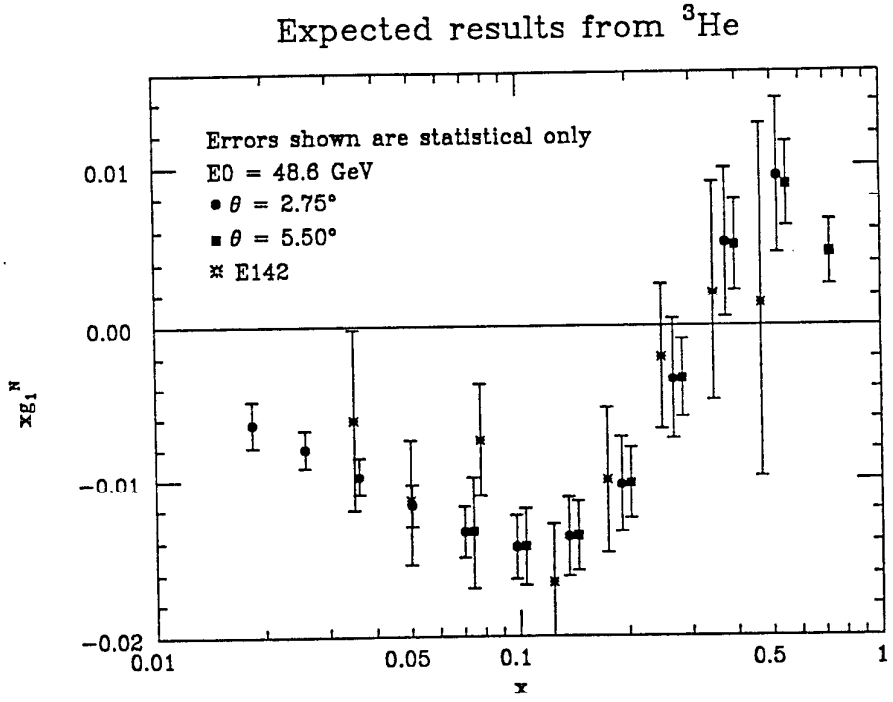

Fig. C-1. Possible results for $xg_1^n(x)$ (statistical errors only) in the 2.75° and the 5.5° spectrometers using ^{3}He target parameters from the E142-x proposal together with E142 data. The possible values for xg_1^n are estimated from a fit to the E142 data given in Appendix B.

REFERENCES

1. J.D. Bjorken, *Phys. Rev.* **148**(1966), 1467, *Phys.Rev.* **D1**(1970), 1376
2. J. Ellis and R.L. Jaffe, *Phys.Rev.* **D9**(1974), 1444, **D10**(1974), 1669
3. SMC, CERN/SPSC 88-47 (1988).
4. B. Adeva *et al*, *Phys. Lett.* **B302**(1993), 533
5. P. L. Anthony, *et al.*, SLAC-PUB-6101, (1993),, *Phys. Rev. Lett.* **71**(1993), 959
6. The EMC collaboration, J. Ashman *et al.*, *Nucl.Phys.* **B328**(1989), 1
7. M.J. Alguard *et al.*, *Phys.Rev.Lett.* **37**(1976), 1261
   , *Phys.Rev.Lett* **41**(1978), 70
8. G. Baum *et al.*, *Phys.Rev.Lett* **51**(1983), 1135
9. C.E. Carlson and Wu-Ki Tung,, *Phys.Rev.* **D5**(1972), 721
10. A.J.G. Hey and J.E. Mandula,, *Phys.Rev.* **D5**(1972), 2610
11. E. Leader and M. Anselmino, *Z.Phys.* **C41**(1988), 239
12. R. L. Jaffe and A. Manohar, *Nucl.Phys.* **B337**(1990), 509
13. R. L. Jaffe and X. Ji,, *Phys. Rev.* **D43**(1991), 724.
14. H. Burkhardt and W.N. Cottingham, *Ann.Phys(N.Y.)* **56**(1970), 453
15. W. Wandzura and F. Wilczek, *Phys.Lett* **B172**(1977), 195
16. V.M. Belyaev and B.L. Ioffe, *Int.J.Mod.Phys* **A6**(1991), 1533
17. R.L. Heimann, *Nucl.Phys.* **B64**(1973), 429
18. R.L. Jaffe and Xiangdong Ji, *Phys.Rev.* **D43**(1991), 726
19. M. Virchaux, A. Milsztajn,, *Phys. Letters* **B274**(1992), 221
20. I.I.Balitsky, V.M. Braun and A. V. Kolnesnichenko,, *Phys. Lett.* **B242**(1990), 245

21. V. D. Burkert and B. L. Ioffe, On the Q^2 variation of spin dependent deep inelastic electron-proton scattering, Preprint CEBAF-PR-92-018 (1992).

22. J. Ellis and M. Karliner, CERN preprint, CERN-TH-6898/93(1993)

23. F. Close, Roberts, preprint RAL 93-04 (1003)

24. M.L. Seely *et al.*, *Nucl.Inst.Meth.* **201**(1982), 303

25. D.G. Crabb *et al.*, *Phys.Rev.Lett* **64**(1990), 2627

26. T.O. Niinikoski and J. M. Rieubland, *Phys.Lett.* **A72**(1979), 141

27. W.W. Ash, Proc. High Energy Physics with Polarized Beams and Targets, Ed. M.L. Marshak (AIP New York 1976) P. 485

28. U. Haertel *et al.* , High Energy Physics with Polarized Beams and Polarized Targets, eds., C. Joseph and J. Soffer, Birkhauser Verlag, Basel (1981) p. 447

29. D.G. Crabb *et al.* , Proc. 4th. Intl. Workshop on Polarized Target Materials and Techniques, Bonn 1984, Ed. W. Meyer, P. 7

30. W. Meyer *et al.*, *Nucl.Instr.Meth.* **215**(1983), 65

31. D.G. Crabb, Proc. High Energy Spin Physics, Bonn 1990, Eds. W. Meyer, E. Steffens, W. Thiel, Springer Verlag 1991, P. 289

32. M. L. Seely et al., Proc. Int. Conf. on High Energy Spin Physics, Brookhaven 1982, ed. G. Bunce, AIP Conf. Proc. 95(1982), 526

33. K. H. Althoff et. al., 4th Intl. Workshop on Polarized target Materials and Techniques, Bonn 1984, Ed. W. Meyer, p. 25.

34. D. Bernstein *et al.,* IEEE Transactions on Nuclear Science, **33**, 86 (1986)

35. P. Amaudruz, *et al.*, *Phys. Lett.* **B295** (1992), 159.

36. D. Wiser, Ph.D Thesis, University of Wisconsin (1977)

37. Private communication from the E142 collaboration.